# Performance Characterization of a 15-cm Ion Thruster with Simulated Beam Extraction

A Thesis

Presented to

The Faculty of the Graduate School

California Polytechnic State University, San Luis Obispo

In Partial Fulfillment

of the Requirements for the Degree

Master of Science in Aerospace Engineering

by

Anup Sanghera

October 2006

AUTHORIZATION FOR REPRODUCTION
OF MASTER'S THESIS

I grant permission for the reproduction of this thesis in its entirety or any of its parts, without further authorization from me.

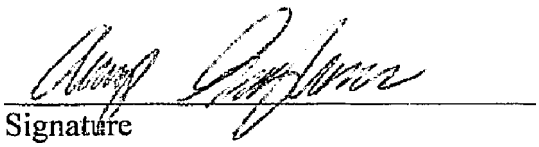

Signature

Oct 30, 2006

Date

APPROVAL PAGE

TITLE: Performance Optimization of a 15-cm Ion Thruster with Simulated Beam Extraction

AUTHOR: Anup Sanghera

DATE SUBMITTED: Oct 30, 2006

Dr. Dianne DeTurris
Adviser

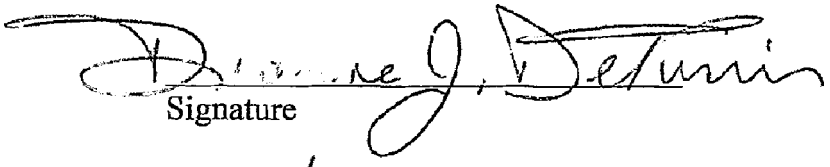

Signature

Dr. Dan Goebel
Committee Member

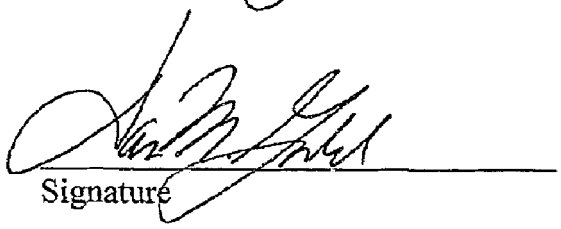

Signature

Dr. Eric Mehiel
Committee Member

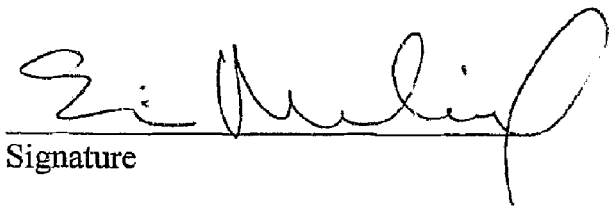

Signature

Dr. Jordi Puig-Suari
Committee Member

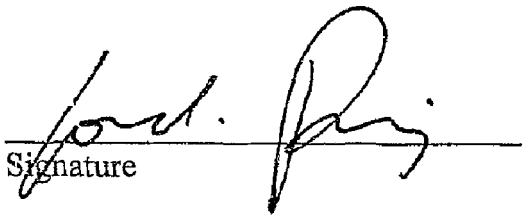

Signature

# ABSTRACT

Performance Optimization of a 15-cm Ion Thruster with Simulated Beam Extraction

Anup Sanghera

In this study the effects of the magnet geometry and the position of the cathode filament were observed on the performance and the beam profiles of a 15-cm ion thruster. A total of five magnet geometries, including the original, were tested and each was tested with 4 different cathode filament positions. The performance of the thruster was determined by finding the performance curves which were plots of the discharge loss vs. the mass utilization efficiency. The beam profiles were found by using a Langmuir probe that was inserted into the discharge chamber immediately upstream of the grids. The study indicated that there was an optimum location for the cathode filament for each of the magnet geometries tested and that the optimum position was approximately the same for all of the magnet geometries. The original magnet geometry had two rings that closed the 22 gauss magnetic contour line. The discharge loss was 131 eV/ion with a mass utilization efficiency of 65% and attained a beam flatness parameter of 0.683. The best performance was measured with the 3 ring configuration which had a discharge loss of 125 eV/ion. The 3 ring geometry closed the 50 gauss magnetic contour line and had a beam profile of 0.705. The worst performance was measured with the 4 ring geometry which had a discharge loss of 151 eV/ion. However, the 4 ring geometry attained the highest beam flatness parameter of 0.739. It was found that there is a trade off between the maximum closed magnetic contour line, the magnetic field free volume inside the discharge chamber, and the number of cusps.

# ACKNOWLEDGEMENTS

I would like to thank my parents, my sister, and my uncle for all their help throughout my life. Without their help I would not be in the position I am today. I would also like to thank all my teachers who have made a difference in my life, because of their hard work and dedication I have been able to achieve all that I have. In addition, I would like to thank Dr. Dan Goebel and Dr. Dianne DeTurris. Dan Goebel's knowledge of the subject matter was invaluable for the completion of my thesis as well as his enthusiasm for the research. Lastly, I would like to thank all my friends for their support.

TABLE OF CONTENTS

LIST OF FIGURES

LIST OF TABLES

# NOMENCLATURE

$A_p$ = Primary electron loss area [$m^2$]
$B$ = Magnetic intensity [T, gauss]
$e$ = Charge [Coulomb]
$f_p$ = Beam flatness parameter
$I_b$ = Beam current [A]
$I_d$ = Discharge current [A]
$I_p$ = Total ion production [particles/second]
$I_{sp}$ = Specific impulse [s]
$\hat{J}_a$ = Ion current to accelerator grid without beam extraction [A]
$\hat{J}_b$ = Ion current leaving the thruster without beam extraction [A]
$J_{b_{simulated}}$ = Simulated beam current [A]
$\hat{J}_d$ = Discharge current without beam extraction [A]
$\hat{J}_g$ = Total grid plane ion current without beam extraction [A]
$j_{i,avg}$ = Average ion current density [$A/m^2$]
$j_{i,peak}$ = Peak ion current density [$A/m^2$]
$L_c$ = Length of cusp [m]
$l_e$ = Electron path length [cm]
$M$ = Mass of ion [kg]
$\dot{m}$ = Flow rate in equivalent amperes [A]
$\hat{\dot{m}}$ = Flow rate in equivalent amperes without beam extraction [A]
$m_e$ = Electron mass [kg]
$n_e$ = Electron density [#/volume]
$n_o$ = Neutral density [#/volume]
$n_p$ = Primary electron density [#/volume]
$r_p$ = Primary electron Larmor radius
$T$ = Thrust [N]
$V$ = Plasma volume [$cm^3$]
$V_b$ = Voltage potential between grids [V]
$V_d$ = Discharge voltage [V]
$\hat{V}_d$ = Discharge voltage without beam extraction [V]
$V_p$ = Potential drop in plasma [V]
$v$ = Velocity of ion [m/s]
$v_e$ = Electron velocity [m/s]

$v_p$ = Primary electron velocity [m/s]

$\Delta V$ = Change in velocity [m/s]

$\eta_d$ = Discharge loss [eV/ion]

$\eta_{d_{simulated}}$ = Simulated discharge loss [eV/ion]

$\eta_m$ = Mass utilization efficiency

$\eta_{m_{simulated}}$ = Simulated mass utilization efficiency

$\phi_i$ = Grid transparency to with beam extraction

$\hat{\phi}_i$ = Grid transparency to without beam extraction

$\sigma_i$ = Ionization cross section

# CHAPTER 1: INTRODUCTION

The use of ion thrusters is increasing as the technology is maturing and becoming more reliable. Ion thrusters are presently being used in earth orbiting satellites and scientific probes. Ion thrusters fall under the classification of electric propulsion, more specifically, they are electrostatic propulsive devices. Electrostatic propulsive devices operate by the acceleration of the charged particles under the influence of electrostatic fields. Ion thrusters offer a high specific impulse ($I_{sp}$) compared to other more traditional propulsive devices. This large increase in $I_{sp}$ is possible since the ions typically exit the thruster at a much higher velocity than the exhaust of typical chemical thrusters. A higher $I_{sp}$ can result in less required propellant mass, which can equate to a lower payload mass for the launch vehicle. The mass saved from reduced propellant can also be used to increase the mass of the payload for increased scientific return or increased commercial output. Thus far the main application for ion thrusters has been station keeping of earth orbiting satellites and scientific probes such as Deep Space 1 and Smart-1. In past NASA programs chemical thrusters have only provided a $\Delta V$ of about 1-4 km/s after launch. Future NASA programs are requiring $\Delta$Vs in the range of 10-30 km/s after launch[1]. To overcome this large discrepancy in $\Delta V$ electric propulsion becomes very attractive since the $I_{sp}$ is order of magnitudes larger (100 times larger) than chemical propulsion. However, usage of ion thrusters is relatively new and there is much research being conducted to increase the performance and lifetime[1-5].

Although ion thrusters are extremely efficient compared to chemical thrusters there is much room for improvement. It is desirable to have a flat beam profile at the exit plane of the thruster and to have a high efficiency. The beam profile refers to the distribution of the ions at the exit plane that are accelerated from the thruster. An uneven distribution of the beam profile causes the grids to deteriorate unevenly and shorten the life of the ion thruster. The magnet geometry is extremely important in influencing the beam profile and also the efficiency of the thruster. It is important to note that in the optimization of the discharge chamber there is a trade off between the beam profile and the efficiency of the thruster. One way to measure the efficiency of the ion thruster is by calculating the performance curves, which consist of the discharge loss versus the mass utilization efficiency.

A 15-cm ion thruster was donated to the Aerospace Engineering Department of Cal Poly, San Luis Obispo by JPL. The objective of this thesis will be to increase the performance of the 15 cm ion thruster. One of the ways to increase the performance of the thruster is to increase the number of ions created in the discharge chamber and to better confine them until they reach the grids and are accelerated. It will be seen if the performance of the thruster can be increased by varying two major components of the thruster which include the cathode filament position and the magnet geometry. The cathode filament will be moved axially and various magnet geometries will be tested to see if the performance can be improved. The 15-cm ion thruster was designed to operate with two magnet rings which confine the plasma. The default geometry has one of the magnet rings located near the cathode and the other is located near the exit plane of the thruster.

The magnetic field geometry for the different cases will be found by using Maxwell SV which is a magnetic and electrostatic-field solver. The cathode filament (electron emitter) will be moved axially to determine at what location the maximum amount of ions can be produced. The magnet geometries will show if the increased magnetic field strength or the increased magnetic field free volume can produce more ions than the default geometry.

Also, the magnet geometry can alter the beam profile at the exit plane of the thruster where the grids are located. A flatter beam profile is desirable for a longer lifetime of the thruster. The beam profiles will be obtained by a Langmuir probe that will be inserted just upstream of the grids in the discharge chamber. The Langmuir probe will obtain readings from multiple positions with a computer controlled traverse mechanism. For the first time at Cal Poly accelerator grids will be added to the thruster; however, there will be no beam extraction but instead simulated beam extraction. Simulated beam extraction will allow optimization of the discharge chamber without the high power consumption necessary for the acceleration of the ions. Simulated beam extraction will also require less propellant flow which will save propellant and will allow for testing to be done in a smaller vacuum chamber (less than $10^6$ to $10^7$ liters/second) because the back pressure will not increase as much[6].

The thruster will be run in a 30 inch bell jar vacuum chamber which can produce a vacuum of $1.6 \times 10^{-5}$ torr. Argon gas will be used because it is less expensive than Xenon

but Xenon propellant will be tested to insure that the trends are consistent. The performance of the ion thruster will be measured by the performance curves.

# CHAPTER 2: BACKGROUND

Consideration of electric propulsion started in the 1950s but it was not until the 1980s and 1990s that major research and development was initiated. More interest was developed as the spacecraft were able to supply the power necessary to run the electric propulsive devices[7]. Hughes has investigated using ion propulsion since the 1960s and initially used the gas cesium. However, since cesium is corrosive, mercury was used instead but mercury also posed a problem because of its environmental impacts. In 1984 Hughes started using xenon because it provided the highest thrust of all gases that did not have any environmental impacts and was inert[8].

Typical chemical thrusters have an Isp of about 200-400 seconds while ion thrusters can have an Isp in the thousands. This basically means that an ion thruster would have to use 10 times less propellant for the same $\Delta V$ requirement that a chemical thruster would. Although ion thrusters have a high $I_{sp}$ compared to chemical propulsive devices they produce very little thrust. The thrust is on the order of mN so the applications are somewhat limited. Electric propulsion devices are different than chemical propulsion devices because electric propulsion devices use an energy source that is independent of the propellant. The energy source is used to ionize the gas and then accelerate the ions to very high velocities[7]. The amount of thrust is related to the amount of power available, this will be shown in section 2.2.1. As a result higher power will mean higher thrust because more ions will be produced and accelerated to a faster velocity[9]. Ion thrusters have so far been used primarily for station keeping to overcome translational and

rotational perturbations. They have been used in north south and east west station keeping for geosynchronous satellites. Ion thrusters have also been used for orbit raising maneuvers[7]. Since ion thrusters have a higher Isp than chemical rockets they need less propellant for a given maneuver. This maneuver may be station keeping of a satellite or escaping earth's gravity for interplanetary space travel. For station keeping of satellites the extra mass that is made available because of the high Isp of the ion thruster can be used for more propellant to increase the lifetime of the satellite. For interplanetary spacecraft the extra propellant could be used to make the spacecraft travel faster than it would with a chemical propulsion system. Ion thrusters are also being investigated for use in precision position missions because thrusts of 0.1micronewtons or smaller are required[1].

## *2.1 Ion Thruster Programs*

The first commercial satellite to carry an ion thruster was PanAmSat-5 in 1997. The ion thruster used on PanAmSat-5 was a xenon ion propulsion system (XIPS) thruster. By 2000 there were 11 satellites in orbit that were using a XIPS thruster. For the Boeing 601 HP and 702 models the XIPS required 90% less propellant for a mission of 12-15 years. The reduced propellant mass has many benefits including a lower launch mass or increased payload mass. XIPS are mainly used for NS or EW station keeping to correct for gravitational forces that take the satellite out of its desired orbit. Once the fuel has been depleted the satellite can no longer operate. Ion thrusters can allow the life of a satellite to be extended because more fuel can be carried. The XIPS on the Boeing 601HP were 13-cm in diameter and the XIPS on the 702 were 25-cm. The Boeing satellites have

four thrusters but only needs two to perform the required maneuvers. In Table 1 the $I_{sp}$, thrust produced, and power required for the 13-cm and 25-cm are shown. The 13-cm has an Isp of 2568 s and a thrust of 18 mN while the 25-cm has an $I_{sp}$ of 3800 and a thrust of 165 mN. The 13-cm thruster requires 500 watts while the 25-cm requires 4500 watts[8].

**Table 1 - Performance of 13 and 25 cm XIPS**

| | Isp (s) | Thrust (mN) | Power Required (W) |
|---|---|---|---|
| 13-cm XIPS | 2568 | 18 | 500 |
| 25-cm XIPS | 3800 | 165 | 4,500 |

The main components of the XIPS thruster are shown in Figure 1. Other than the thruster the main components are the propellant tank and the power processing unit (PPU)[8]. The neutralizer can also be seen but will be discussed in the next section.

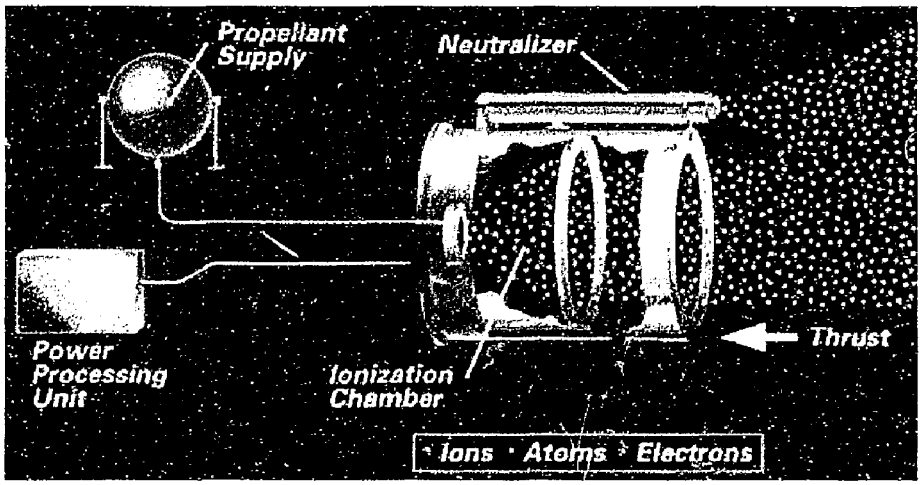


**Figure 1 - XIPS Thruster and Major Components[8]**

The first deep space mission to use an ion thruster was Deep Space 1, which launched on October 24, 1998[10,11]. Before Deep Space 1 all the missions that had used an ion thruster

were earth orbiting satellites. Part of the New Millennium Program (NMP) designed to develop and validate high risk and high benefit technologies a NASA Solar Electric Propulsion Technology Application Readiness (NSTAR) ion thruster was used as the primary means of propulsion for Deep Space 1[12]. The 30 cm NSTAR ion thruster was one of the 12 new technologies being tested which had an $I_{sp}$ of 3100 s at a thrust of 20-92 mN[10,13]. The NSTAR engine operates over a power range of 0.5 kW to 2.3 kW[14]. The NSTAR engine utilized a hollow cathode for producing the electrons to ionize the Xenon and the positively charged ions were electrostatically accelerated with a potential of 1280 V through two molybdenum grids which accelerated the ions to approximately 31.5 km/s[12,13]. The system also consists of a power processor and digital control and interface units[10]. The NSTAR thruster successfully fired for over 16,200 hours for trajectory correction maneuvers and tests. The thruster consumed a total of 72 kg of Xenon and providing the spacecraft with a total $\Delta V$ of 4.5 km/s[10, 15]. A view of Deep Space 1 can be seen in Figure 2.

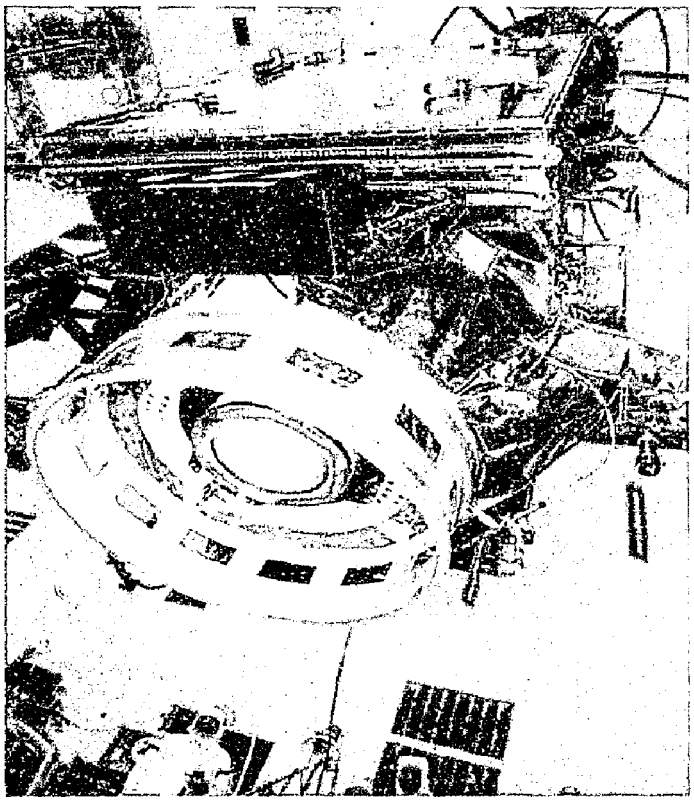

**Figure 2 - Deep Space 1[10]**

The next NASA spacecraft that will use an ion thruster is the Dawn spacecraft scheduled to launch on June 20, 2007[16]. The DAWN spacecraft will also use the NSTAR thruster that will have the same performance as the Deep Space 1 ion thruster. The DAWN Ion Propulsion System will provide the spacecraft with a $\Delta V$ of about 10km/s[1]. DAWN's mission is to visit two of the largest protoplanets, Ceres and Vista, which are located between Mars and Jupiter in the asteroid belt[17].

The first European spacecraft to have electric propulsion as the primary propulsion system was SMART-1. Small Missions for Advanced Research in Technology (SMART) was part of the European Space Agency's Horizons 2000 scientific program[18].

One of the more ambitious electric propulsion programs was NASA's Prometheus with the Nuclear Electric Xenon Ion System (NEXIS) ion thrusters. The program was required to operate at power levels of 16 to 20 kW with specific impulses in the range of 6000 to 7500 seconds with burn times of over 10 years[19].

## *2.2 Theory*

In a theoretical and practical sense ion thrusters are extremely complicated. A great deal of research is being conducted to make the thrusters more efficient, more powerful, and operate longer[2-5, 20-22]. The magnetic field geometry of the thruster plays a critical role in the efficiency and beam profile of the thruster. Since simulated beam extraction was used in this experiment, fundamental background information is provided in this chapter. The theory of plasma diagnostics, using Langmuir probes, is also presented in this chapter.

### 2.2.1 Principles of Ion Thrusters

Ion thrusters are a form of electric propulsion which uses electrostatic fields to accelerate ionized particles. Ions are atoms that have an electrical charge and the process of ionization is electrically charging an atom by adding or removing an electron. The gas can be ionized in multiple ways including DC electron discharges and RF discharges. In most ion thrusters that have been used and studied thus far DC electron discharges have been used. Thrusters that use DC electron discharges are called electron bombardment thrusters and the electrons are generated by a hollow cathode[10]. Figure 3 shows a basic layout of the thruster.

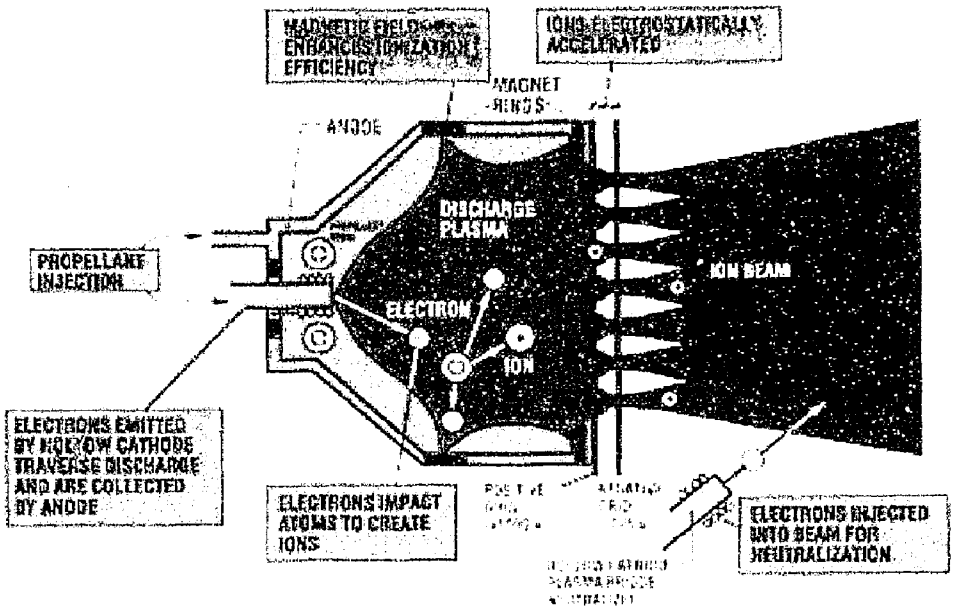


Figure 3 - Ion Thruster with Components[23]

The electrons that are extracted into the discharge chamber from the hollow cathode, which are called primary electrons, are attracted to the positive potential of the anode. As the electrons are attracted to the anode they collide with gas atoms and ionize them by removing an electron. To prevent the electrons to travel from the cathode directly to the anode wall magnetic fields are used in the discharge chamber to confine them. This also increases the path length of the electrons and increases the chances that the electron will ionize an atom which increases the ionization efficiency[24]. At the exit plane of the thruster are 2 or 3 grids, or ion optics, that accelerate the ions to high speeds. The upstream grid is called the screen grid and the downstream grid is called the accelerator grid. The screen grid is usually connected to the cathode potential to provide confinement to the electrons that are in the discharge chamber[24]. Once the ions pass through the screen grid they encounter a large voltage potential between the screen grid and the accelerator grid causing the ions to accelerate. The ions that go through apertures in the accelerator

grid form many streams of ions and together they form an ion beam[25]. The velocity of the ions in the ion beam can be increased by changing the voltage between the screen grid and the accelerator grid. This can be seen in Equation 1

$$v = \sqrt{\frac{2eV_b}{M}} \qquad \text{Equation 1}$$

where e is the charge, M is mass of the ion, and $V_b$ is the total voltage that the ions are accelerated through. From Equation 1 it can be seen that there is no limit to how fast the ion can leave the thruster. Typically the ions are accelerated to a speed of about 30 km/s[23]. It is important to note that because ions are leaving the thruster there is a charge imbalance. As a result negative charge also has to be expelled from the thruster. Negative charge is expelled with the use of a neutralizer which is essentially another hollow cathode and emits electrons.

The thrust produced by an ion thruster can be found by Equation 2.

$$T = I_b\sqrt{\frac{2MV_b}{e}} \qquad \text{Equation 2}$$

In Equation 2 e is the charge and $I_b$ is the beam current in amps.

To determine the behavior of the discharge chamber performance curves (plots of discharge loss versus mass utilization efficiency) are found. The discharge loss is the electrical cost of producing beam ions and the mass utilization efficiency is the percentage of the propellant that becomes ionized. These curves show how well the plasma generator functions[24]. The discharge loss can be found by using Equation 3 and the mass utilization efficiency can be found by using Equation 4.

$$\eta_d = \frac{I_d V_d}{I_b} \qquad \text{Equation 3}$$

$$\eta_m = \frac{I_b}{e\dot{m}} \qquad \text{Equation 4}$$

In Equation 4 $\dot{m}$ is in particles per second.

The $I_{sp}$ of an ion thruster is found in a similar calculation as for chemical thrusters but the inefficiencies of the ion thruster must be taken into consideration. Equation 5 shows how to calculate the $I_{sp}$ of an ion thruster.

$$I_{sp} = \frac{v\eta_m}{g} \qquad \text{Equation 5}$$

To compare the different magnet geometries quantitatively the following equations were used. Equation 6 calculates the area where the primary electrons are lost to the anode wall due to the cusps; the primary electron loss area is given by

$$A_p = 2r_p L_c \qquad \text{Equation 6}$$

where $r_p$ is the primary electron Larmor radius and $L_c$ is the length of the cusp. A smaller $A_p$ is desirable since it represents the area where the primary electrons are lost. The Larmor radius refers to the path of a charged particle moving in a magnetic field and is given by

$$r_p = \frac{1}{B}\sqrt{\frac{2m_e V_p}{e}} \qquad \text{Equation 7}$$

where B is the magnetic strength, $m_e$ is the mass of the electron, $V_p$ is the potential drop in the plasma, and e is the charge. The Larmor radius can also be calculated for ions and it can be seen that more massive ions will have a larger Larmor radius. Furthermore, the Larmor radius is larger in lower strength magnetic fields as shown by Equation 7.

Another important quantitative measure is the electron path length, which is calculated by

$$l_e = \frac{V}{A_p} \qquad \text{Equation 8}$$

where V is the plasma volume and $A_p$ is the primary electron loss area. A larger electron path length is desired since it increases the chance that the electron will collide with a neutral atom and ionize it.

The beam profiles were quantified by Equation 9. The beam flatness parameter, $f_p$, was found by dividing the average ion current density by the peak ion current density at the grids and is a unit less number.

$$f_p = \frac{j_{I,avg}}{j_{I,peak}} \qquad \text{Equation 9}$$

It is desirable to have the beam flatness parameter as close to 1 as possible because it indicates a flatter beam profile.

### 2.2.2 Simulated Beam Extraction

As the technology for ion thrusters is advancing ion thrusters are requiring more power to operate and test. Thrusters are requiring 10's of kilowatts for operation and 1000's of hours of life testing in vacuum chambers. As a result of the high power needed to extract a beam it would be desirable to optimize the discharge chamber without an actual beam extraction. Beam extraction refers to ions actually being accelerated from the ion thruster. This idea of a simulated beam extraction, where ions would not be accelerated by applying a large voltage to the grids, was explored by John Brophy from JPL[6]. Brophy determined that the ion transparency decreased without beam extraction from 0.8 to 0.22 for the standard J-series thruster ion optics. Ion transparency is the percentage of ions that travel to the accelerator system that become ions in the exhaust beam. The ions that do not become part of the exhaust beam recombine with electrons on the grid surface. An ion transparency of 0.8 can be obtained with beam extraction even though the physical open area of the J-series screen grid is 67%. The ion transparency of 0.8 is possible because of focusing effects that result from the applied voltage to the grids. With simulated beam extraction there are no high voltages applied to the grids which greatly reduces the ion transparency. As a result more ions hit the grid surface and do not go through the grid apertures. The ions that strike the grid surface recombine with electrons and thus become neutral atoms. These neutral atoms will either return into the discharge chamber or will exit the thruster. If the same flow rate that is used with beam extraction is used without beam extraction the neutral atom density inside the discharge chamber will increase. Therefore, in order to simulate beam extraction the flow rate must be reduced. This reduction in flow rate is desirable because significantly less propellant will be

required which will also reduce costs to operate the thruster. Furthermore, since a lower flow rate is used the testing can be done in smaller and cheaper vacuum chambers. Simulated beam extraction allows testing and optimization to be done much more efficiently because less power, less propellant, and smaller vacuum chambers can be used[6].

Studies have been conducted where discharge chamber optimization was performed without beam extraction; however, when those discharge chambers were tested with beam extraction they were found to perform much worse in terms of performance[6]. Brophy states that the discrepancy might be the result of the neutral atom density decreasing when there is a beam extraction. It is also known that the performance of the discharge chamber is dependent on the neutral atom density. The discharge chamber performance is also related to the ion density distribution. In order to match discharge chamber performance with and without beam extraction it is important that the neutral atom density and the ion density are the same with and without beam extraction. As stated earlier the ion transparency is reduced when the high voltages are removed from the grids. This reduction in ion transparency increases the neutral atom density. As a result the propellant flow rate into the discharge chamber must be decreased for operation without beam extraction. The relationship between the mass flow rate with and without beam extraction is shown in Equation 10.

$$\hat{\dot{m}} = \dot{m}\left[1-\eta_m\left(1-\frac{\hat{\phi}_i}{\phi_i}\right)\right] \qquad \text{Equation 10}$$

In Equation 10 $\dot{m}$ is the total flow rate with beam extraction, $\eta_m$ is the mass utilization efficiency, $\phi_i$ is the ion transparency with beam extraction, $\hat{\phi}_i$ is the ion transparency without beam extraction, and $\hat{\dot{m}}$ is the mass flow rate without beam extraction. The equation shows that given a mass flow rate with beam extraction and mass utilization efficiency the mass flow rate without beam extraction is a function of the ratio of the ion transparency with and without beam extraction.

To find the effective accelerator system transparency to ions without beam extraction Equation 11 was used, where it is assumed that 55% of the ions which strike the grid leave the thruster.

$$\hat{\phi}_i = \frac{.55\hat{J}_a + \hat{J}_b}{\hat{J}_g} \qquad \text{Equation 11}$$

To calculate the beam current with beam extraction it is assumed that the beam current can be calculated by using $\hat{J}_g$ (the total ion current to the grid) and the ion transparency with beam extraction, as shown in Equation 12.

$$J_{b_{simulated}} = \phi_i \hat{J}_g \qquad \text{Equation 12}$$

To obtain the simulated mass utilization efficiency Equation 10 and Equation 12 can be rearranged. The equation to find the simulated mass utilization efficiency is shown in Equation 13.

$$\eta_{m_{simulated}} = \frac{\phi_i \hat{J}_g}{\hat{m} + \phi_i \hat{J}_g \left(1 - \frac{\hat{\phi}_i}{\phi_i}\right)}$$ Equation 13

The total mass flow rate is in equivalent amps. The simulated discharge loss, which is also known as the beam ion energy cost, can be found by using Equation 14.

$$\eta_{d\ simulated} = \frac{\left(\hat{J}_d - \phi_i \hat{J}_g\right)\hat{V}_d}{\phi_i \hat{J}_g}$$ Equation 14

In this experiment performance curves were obtained by fixing the total mass flow rate and the discharge voltage and varying the discharge current and consequently the total ion current at the grids. Simulated beam extraction has been used in numerous experiments and provides similar performance numbers to actual beam extraction[26, 27].

### 2.2.3 Magnetic Field Geometry

The magnetic field prevents the electrons from traveling directly to the anode after they are emitted from the cathode and confines the plasma until it reaches the grids. The design of the magnetic field is crucial for the performance of the thruster and has effects on the efficiency of the thruster as well as the beam profile. Today there are two types of magnetic field geometries that are used; they include the multipole magnetic field for ring cusp thrusters, and divergent solenoidal magnetic fields for Kaufman thrusters. For ion thrusters the magnetic rings provide magnetic confinement of the electrons with some loss at the magnetic cusps[28]. The cusp refers to where the field lines intersect the magnet face, since the magnet rings are a collection of smaller magnets a magnet ring is a cusp. Figure 4 shows a cross sectional view of the 15-cm ion thruster with the magnets and the body of the thruster. The figure shows the magnetic fields lines which were generated by Maxwell. Since each magnet ring is a cusp more magnet rings result in more cusps.

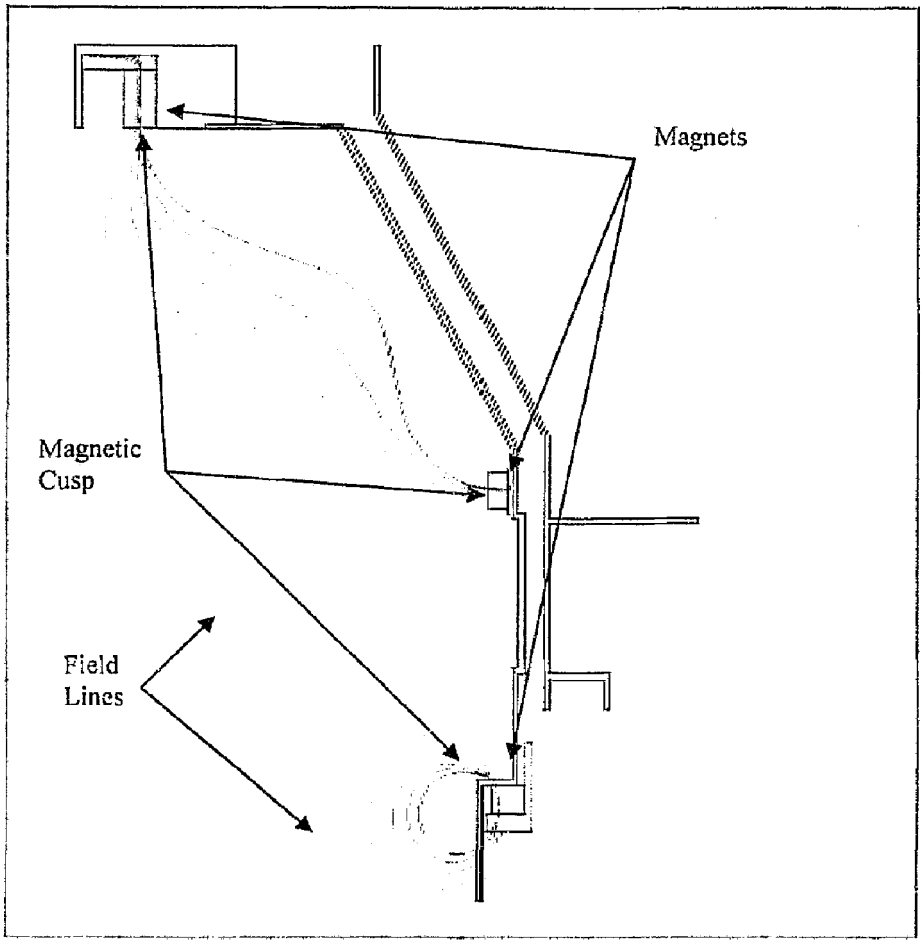


**Figure 4 - Magnetic Cusps**

There are multiple aspects of the magnetic field geometry that must be considered to improve the performance of the ion thruster. One is the magnetic field strength that closes the contour inside the discharge chamber. Typically a higher magnetic field strength that closes the contour inside the discharge chamber will yield higher performance. In most ion thrusters the closed magnetic contour is about 20-50 gauss. However, if the design is strictly based on the magnetic strength that closes the contour the consequences may include either a decrease in the magnetic field free volume or excessive losses at the magnetic cusps. The magnetic field free volume refers to the region in the thruster where the magnetic field does not affect the plasma; a large magnetic field free volume is

desired. A large volume is desired because the ionization rate is proportional to the volume. The relationship between the amount of ions produced and magnetic field free volume is shown below in Equation 15.

$$I_p = n_o n_e \langle \sigma_i v_e \rangle V + n_o n_p \langle \sigma_i v_p \rangle V \qquad \text{Equation 15}$$

where $n_o$ is the neutral atom density, $n_e$ is the plasma electron density, $n_p$ is the is the primary electron density, $\sigma_i$ is the ionization cross section, $v_e$ is the plasma electron velocity, $v_p$ is the primary electron velocity, and V is the magnetic field free volume (also known as the plasma volume)[24]. The plasma volume is defined to be inside the last closed contour up to the 50 gauss closed magnetic contour line. One gauss is equal to 0.0001 tesla; tesla is a unit of measurement used to define the intensity of a magnetic field. A closed magnetic contour line refers to a contour of constant magnetic strength. Figure 5 shows an example of a 50 gauss closed magnetic contour line and a 60 gauss open magnetic contour line. The closed magnetic contour line forms a pocket within the discharge chamber.

A magnet geometry consisting of three rings, or cusps, will be used as an example with the 15-cm thruster. The Maxwell SV software was used to model the magnetic field inside the discharge chamber. Figure 5 shows the standard three ring geometry and strengthened three ring geometry. Figure 5 shows that the standard three ring geometry closed the 50 gauss magnetic contour line. However, if it was desired to increase the strength of the closed magnetic contour line it would be necessary to either strengthen the

magnets or add another magnet ring, both of which could have adverse performance impacts.

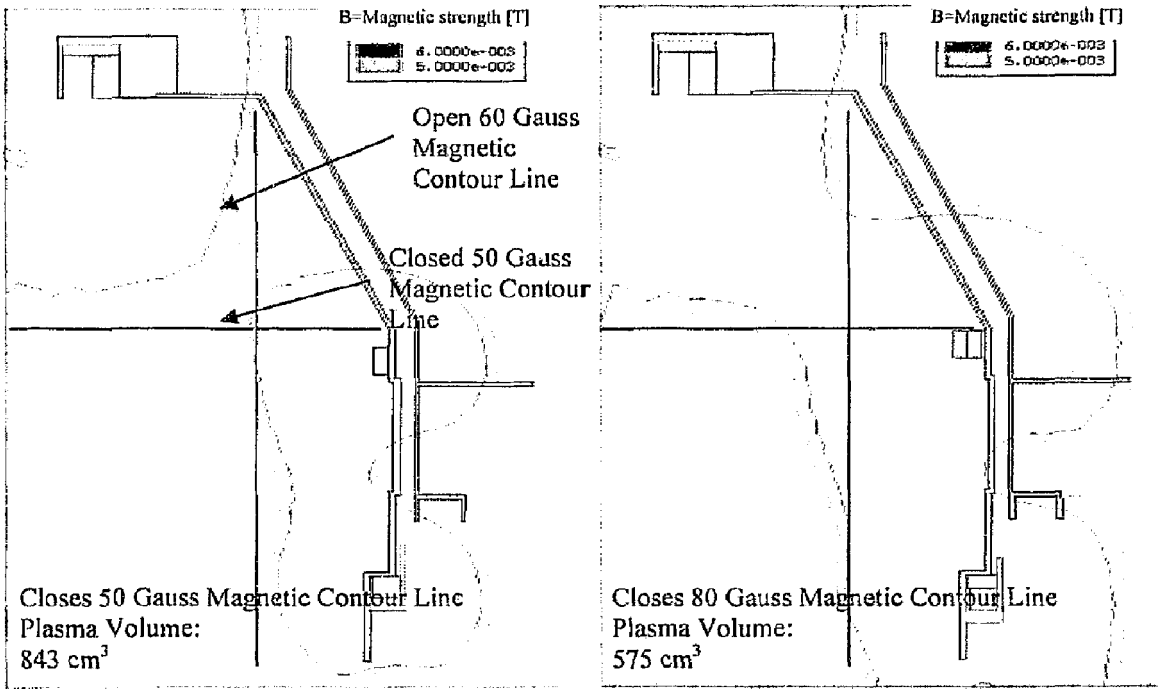


**Figure 5 - Comparison of 3 Ring Geometry (Left) and Strengthened 3 Ring Geometry (Right)**

The black lines are used for comparison purposes to show how the 50 gauss magnetic contour line changes. The strengthened three ring geometry closed the 80 gauss magnetic contour line; however, the plasma volume decreased since the 50 gauss magnetic contour line moved closer to the axis of thruster as shown in Figure 5. The plasma volume for Figure 5 (left) was 843 $cm^3$ and the plasma volume for Figure 5 (right) was 575 $cm^3$.

To increase the strength of the closed magnetic contour line without reducing the plasma volume more magnet rings must be added. Figure 6 shows a comparison of three ring geometry and five ring geometry magnetic fields. The five ring geometry closed the 180 gauss magnetic contour line. A closure of the 180 gauss magnetic contour line is not used

in actual ion thrusters because there is no significant benefit from such a high strength, but is used here for comparison purposes.

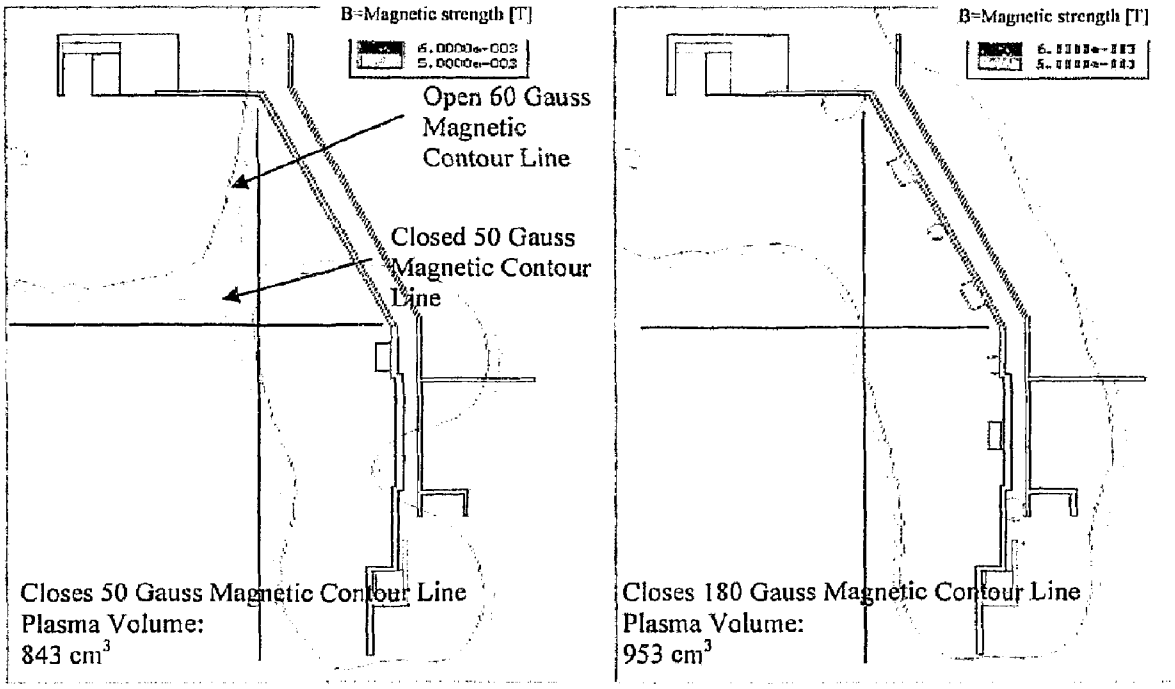


**Figure 6 - Comparison of 3 Ring Geometry (Left) and 5 Ring Geometry (Right)**

Even though the closed magnetic contour line significantly increased, the plasma volume did not decrease; in fact it increased, as shown in Figure 6. The addition of magnet rings results in the magnetic contour lines being pulled in closer to the anode. However, ions and electrons are lost at the cusps and increasing the number of cusps results in a decrease in performance. The plasma volume for Figure 6 (left) was 843 $cm^3$ and the plasma volume for Figure 6 (right) was 953 $cm^3$. Figure 5 and Figure 6 show there is a trade off between the closed magnetic contour line, plasma volume, and the number of cusps.

A property of the magnetic field that is not always taken under consideration is the magnetic field line geometry[28]. A study of the magnetic field line shape and its effects on the efficiency and the beam flatness was conducted by Richard Wirz and Dan Goebel at JPL. Figure 7 shows the basic layout of the NSTAR thruster. The lines with the arrows represent the magnetic field lines and the colored lines represent the magnetic strength contours. The magnetic strength contour is shown to display the movement of the magnetic minimum for the different magnet geometries. The baseline NSTAR thruster had a large region of magnetic field lines that were parallel to the thruster axis (axial field lines) because of over confinement, as shown in Figure 7. The consequence of the axial field lines was a peak in ion density near the center of the exit plane.

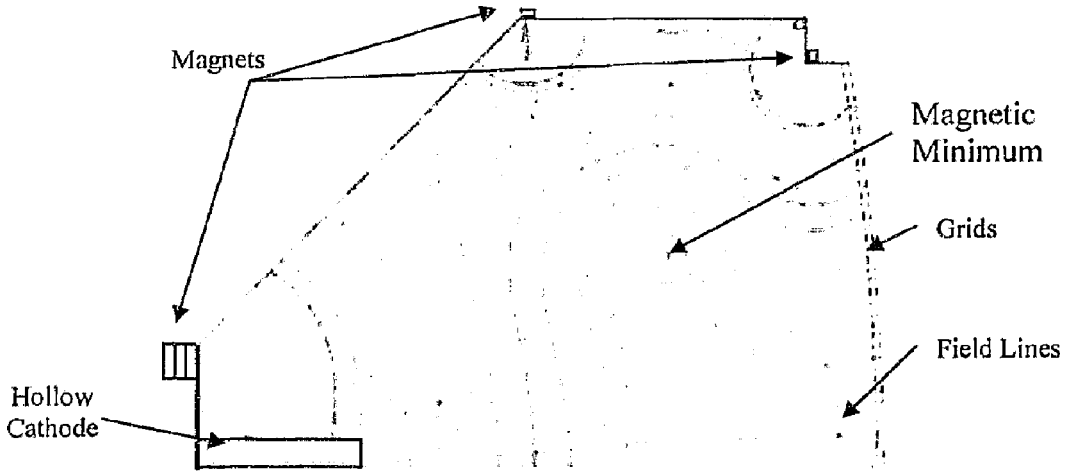


**Figure 7 - NSTAR Baseline[28]**

Figure 7 shows how the magnetic minimum diverts the field lines around it and moving the magnetic minimum closer to the axis could reduce the axial field lines. To move the magnetic minimum the middle magnet ring was strengthened as shown in Figure 8. By

strengthening the middle magnet ring the magnetic minimum was moved closer to the axis and the magnetic strength of the field line that closed the contour increased[28].

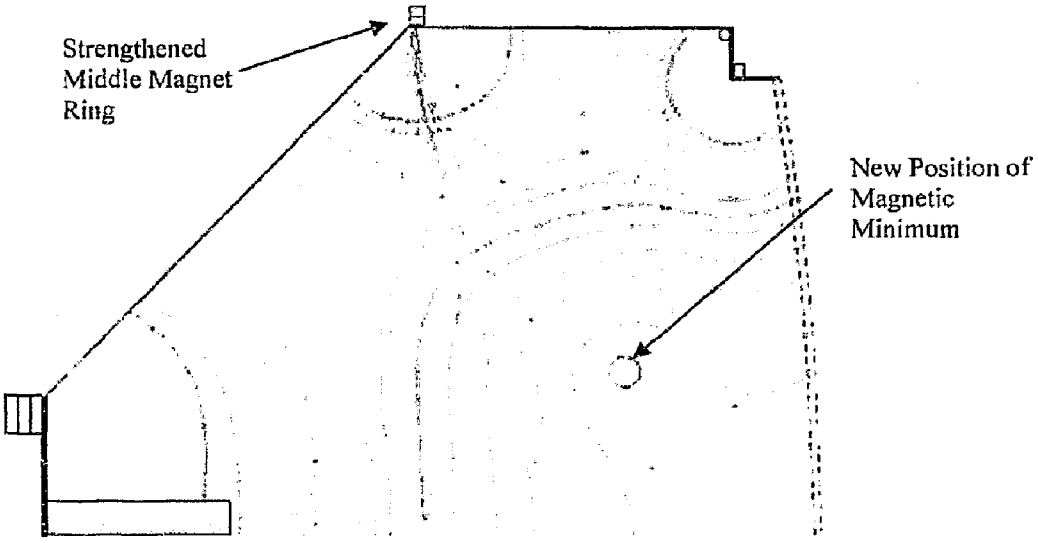


**Figure 8 - Magnetic Field of Strengthened Middle Ring of NSTAR[28]**

Figure 8 shows that by moving the magnetic minimum closer to the axis the axial field lines were reduced. The strengthened middle magnet ring produced a flatter beam profile than the geometry shown in Figure 7 because of the reduced axial field lines[28].

The study also found that a magnetic field designed with 4 magnetic rings, if designed correctly, could eliminate the field lines that run from the cathode to the grids. With the NSTAR thruster the fourth magnetic ring produced a magnetic field where the field lines that were emanating from the cathode connected with the magnet ring near the exit plane and not the grids. With the fourth ring there were two magnetic minimums inside the discharge chamber. Figure 9 shows one magnetic minimum near the axis of the thruster and the other off axis.

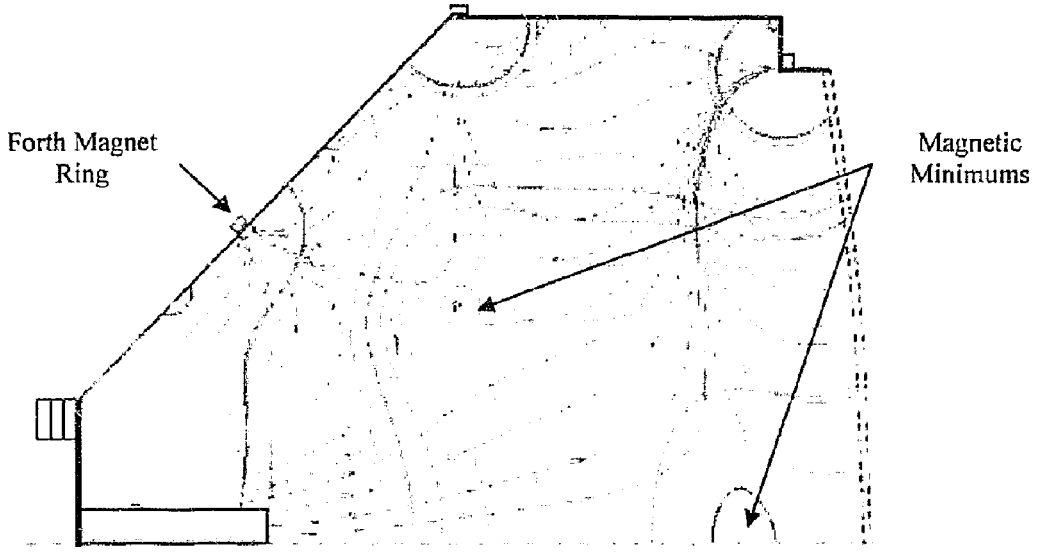


**Figure 9 - Magnetic Field of NSTAR Thruster with 4 Rings[28]**

The magnetic minimum near the axis caused the field lines to diverge from the grids. The study concluded that the magnetic field line shape must guide the primary electrons from the cathode to off axis points where they can ionize the propellant. On-axis confinement of the primary electrons must be avoided to obtain a flat beam profile. Thrusters with four magnet rings inherently have an on-axis magnetic minimum and thrusters that have three magnetic rings can have a magnetic minimum near the axis by strengthening the middle magnet ring. The magnetic field strength that closes the contour inside the discharge chamber must be high enough to have good performance but low enough to allow a stable discharge[28].

## 2.2.4. Plasma Diagnostics

In this experiment the beam profile will be measured using a Langmuir probe. It is important that the data is collected in such a fashion that the plasma in the discharge chamber is not disturbed by the probe. Langmuir probes are often used in plasma physics to spatially resolve plasma parameters in low-temperature plasmas and are one of the most widely used probes in plasma characterization[20, 29]. The Langmuir probe is an electrostatic device that has a voltage applied to it by an external power supply and is usually biased with the cathode common or the anode. The probe is usually in the shape of a cylinder or a flat disk. The Langmuir probe used in this project is discussed in section 5.3. The plasma properties that can be determined are electron temperature, ion and electron saturation currents, and plasma density. As the voltage on the probe is varied the corresponding current is obtained at each voltage. The plot of the current and the voltage is called the I-V curve. An example of an I-V curve is shown in Figure 10. In Figure 10 the red vertical lines divide the curve into three distinct regions.

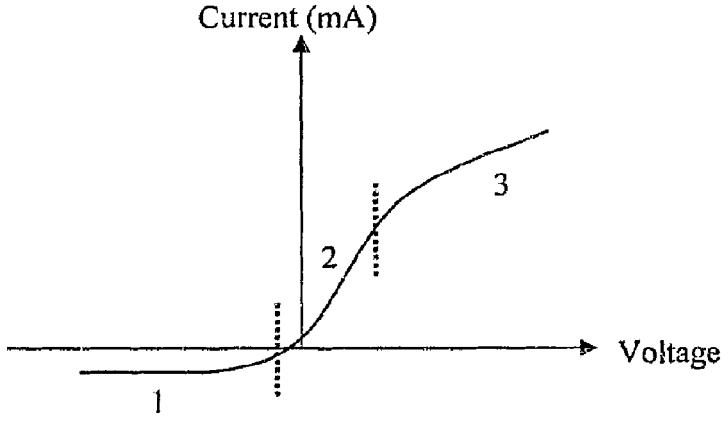


**Figure 10 - I-V Curve**

There are three distinct regions for the I-V curve. Region 1 is found when the probe voltage has a large negative potential such that the current of ions saturates. In this region there is no current from the electrons because they are repelled by the negative potential. As the voltage on the probe is increased positively the current of ions decreases and the current of electrons increases. At the point the two currents are equal the current collected by the probe is 0 and the voltage at this point in known as the floating potential. This is also the start of region 2 which is the retarding region. As the voltage increases more electrons are collected by the probe and eventually the electron current saturates. However, a sheath forms around the probe which increases the area that can collect the electrons as the voltage is increased with a cylindrical probe. Therefore actual electron saturation current is not obtained. If a flat disk is used a sheath still forms but the growth is perpendicular to the surface so the collection area does not increase[20]. In this experiment the ion saturation current (Region 1) was used to determine the ion current beam profile at the exit plane directly upstream of the screen and accelerator grids.

# CHAPTER 3: 15-CM THRUSTER

The 15-cm ion thruster was donated by JPL. The ion thruster was not designed for spaceflight but was used in laboratory testing at JPL. The thruster is entirely non-magnetic except for the magnets and the components that hold the magnets. This is so the magnetic field is primarily influenced by the magnets. Figure 11 shows a cross sectional view of the 15-cm ion thruster with the original magnet configuration.

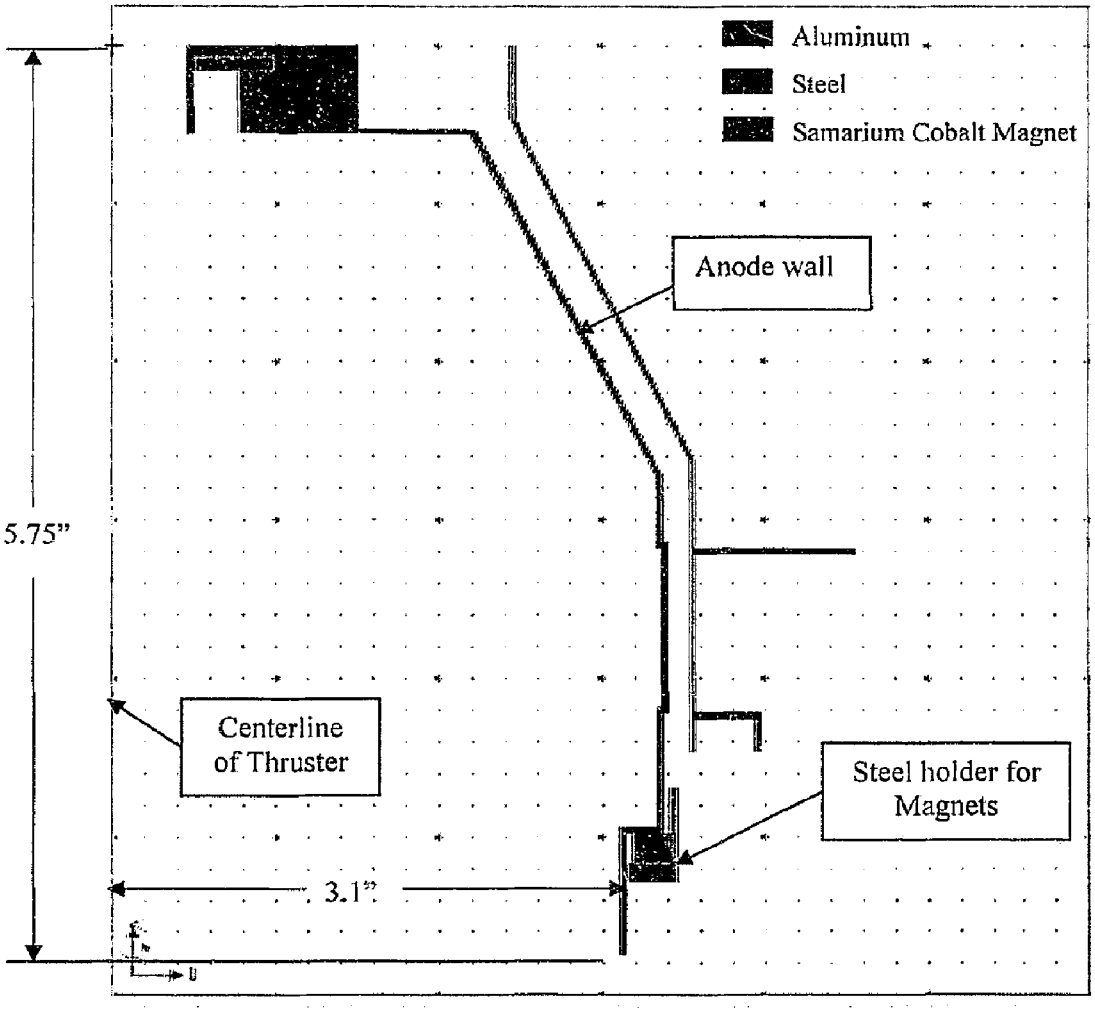


**Figure 11 - 15-cm Ion Thruster Schematic**

## 3.1 Cathode

The thruster did not come with a cathode or a cathode holding device so one was designed and manufactured. There were three requirements for the cathode holder, be able to move the cathode filament axially, be electrically isolated from the anode, and to hold the cathode filament. To fulfill the requirements, threaded rods which were 4 inches long were used in conjunction with internally threaded ceramic cylindrical pieces. The rods were a #6-32 thread type. The ceramic standoffs would electrically isolate the threaded rods from the anode and were a ¼" in long and ¼" inch in diameter with #6-32 threads. Since the ceramic pieces were threaded the end of the rods could be positioned anywhere in the thruster axially. To hold the cathode filament securely small holes were drilled near the end of the threaded rods. The holes were drilled so that a #1-70 screw could be inserted and were fastened with a nut on the other end. Two washers were used to securely hold the tungsten filament on each rod.

Figure 12 shows the components of the cathode system and their arrangement. In the figure only two of the four ceramic standoffs can be seen. The cathode plate was screwed on to the thruster to securely fasten it.

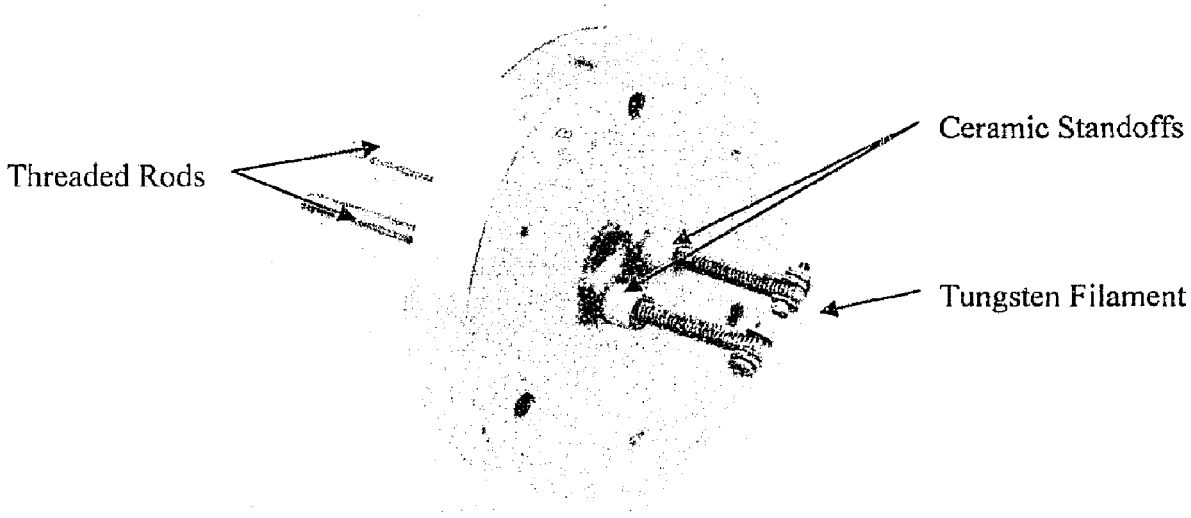


**Figure 12 - Cathode Setup**

A close up view of the filament being held in place at the end of the threaded rod can be seen in Figure 13. In the previous thesis by Randy Yount the tungsten filament was placed into holes at the end of the rod[30]. This proved to be very difficult because when the voltage was applied and current was running over the tungsten wire there were fluctuations in the discharge current. The fluctuations were the cause of the tungsten wire not being securely fastened. With the current design the washers that are on either side of the filament securely hold it in place when the nuts are tightened for each end. As a result the fluctuations no longer persisted.

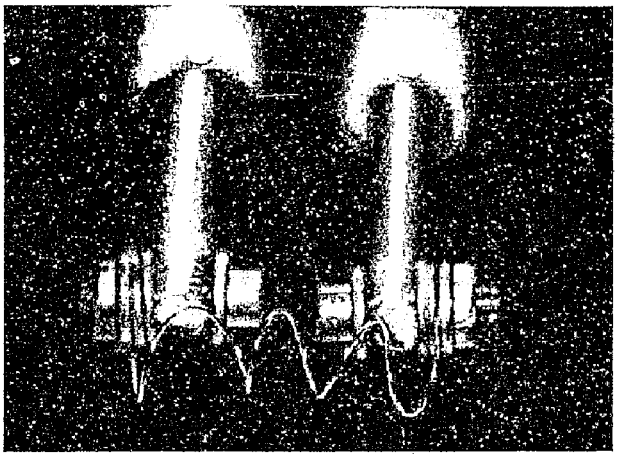

**Figure 13 - Close-Up View of Tungsten Filament**

## *3.2 Fuel Connections/Manifold*

The fuel manifold is located about halfway between the cathode magnet ring and the exit plane of the thruster. This location for the fuel manifold is much different from the 13 cm XIPS thruster where its fuel manifold is located near the cathode magnets. The fuel manifold is shaped like a ring with a thickness of 0.25 in and a diameter of about 15 cm. There are small openings in the fuel manifold every 60 degrees with a total of six holes. The fuel manifold connector was fitted with a Swagelok connection so that the thruster could be integrated with the existing fuel line connection as shown in Figure 14.

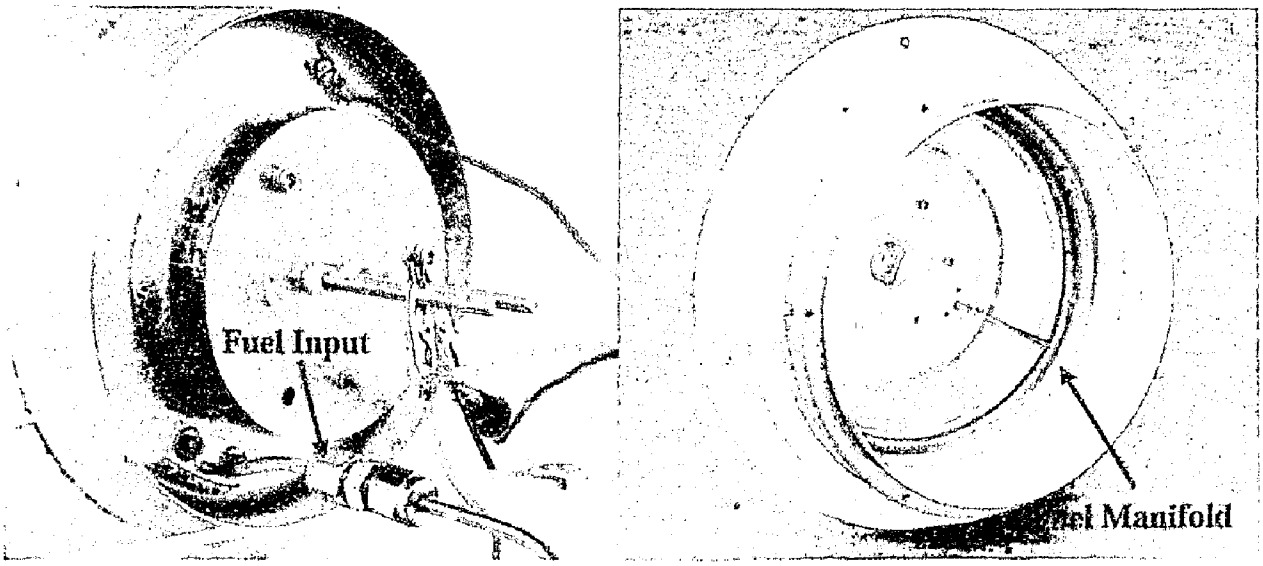


**Figure 14 – Fuel Connection and Fuel Manifold**

From Figure 14 it can also be seen that the fuel line goes through the back end of the thruster near the cathode plate. The fuel line connects to the fuel manifold on the inside of the thruster and has a diameter of 0.125 inches.

## *3.3 Grids*

To run the experiment accurately, accelerator grids were used instead of a simulator plate which was used previously at Cal Poly. The grids are made of carbon and attach to the thruster near the exit plane. The grids were attached to a graphite frame which was attached to the steel circular frame that also holds the magnets. It's important to note that there should be no gap or exposed area between the screens and the thruster because the neutral density will decrease and thus change parameters of the thruster. The grids are shown in Figure 15. There are two grids that attach to the exit plane of the thruster, the

upstream grid is called the screen grid and the down stream grid is called the accelerator grid. The individual grid hole size was about 0.04" in diameter and the grid plate diameter was about 8".

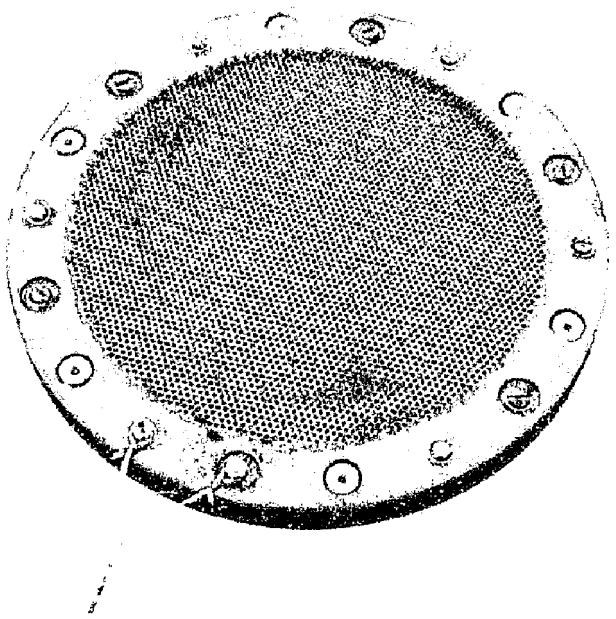

Figure 15 - Grids

From Figure 15 the wires that place the negative potential on the grids can also be seen. The wires were intentionally shorted because both the screen grid and accelerator grid have the same voltage applied to them and the current from the screen grid and the accelerator grid were measured as one current which represented the ion current to the grids. The grids are not at different voltages since the beam extraction is being simulated.

## 3.4 Original Magnet Geometry

The original magnet geometry of the thruster included two rings, one near the cathode and other near the exit plane of the thruster. The magnetic ring that is located near the exit plane of the thruster is enclosed in a steel circular frame that attaches to the thruster with 6 #4-40 screws. Samarium Cobalt magnets were used because they retain their magnetic strength in high temperatures. The magnets that came with the thruster measured 0.475 x 0.23 x 0.195 inches. Since one of the main items being testing in this experiment is the magnetic field of the thruster additional magnets were purchased and placed in various orientations. The magnets that were purchased were 0.5 x 0.25 x 0.125 inches. The magnets were samarium cobalt grade 24 magnets and purchased from K & J Magnetics. The other magnet geometries are shown and discussed in the Testing and Procedure section. Figure 16 shows the shapes and sizes of the different magnets.

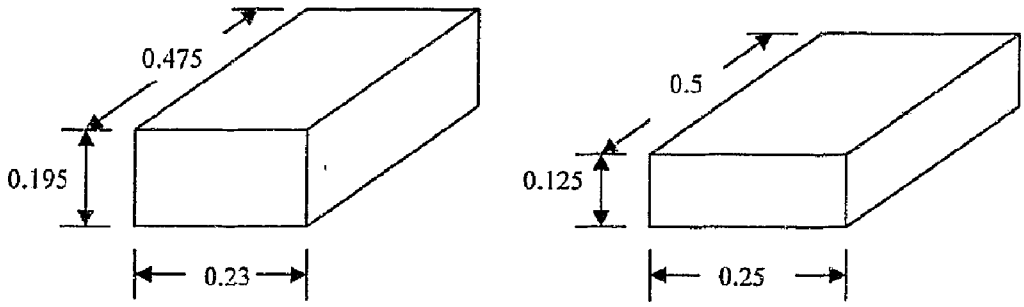


**Figure 16 - Original Magnets (left) and Purchased Magnets (right)**

# CHAPTER 4: EXPERIMENTAL SETUP

Testing of the 15-cm ion thruster was performed in Cal Poly's Aerospace Engineering Department's Aerothermodynamics Laboratory. The laboratory provided compressed air and water both of which were necessary for the experiment. The facility housed the 30 inch bell jar vacuum chamber that was to be used in the experiment to simulate conditions of space. Other equipment included pumps, bell jar hoist, power supplies, fuel supply equipment, and a traverse.

## *4.1 Vacuum Chamber*

The vacuum chamber was manufactured by High Vacuum Equipment Corp of Hingham Massachusetts and was donated to Cal Poly by Stanford University in 2000[31]. The inside diameter of the vacuum chamber is about 30 in. The vacuum chamber is shown in Figure 17.

A helium leak detector was used to find leaks in the vacuum chamber and leaks were found. Most of the fixes included adding new o-rings but also the removal of the previous mechanical traverse system. Fixing the leaks lowered the base pressure slightly but the more important benefit was that the chamber pumped down in about half the time as before the fixes.

**Figure 17 - Vacuum Chamber**

Two students set up the vacuum chamber as a senior project so that it could be used by other students who needed operating conditions of space[32]. A schematic of the vacuum chamber can be seen in Figure 18.

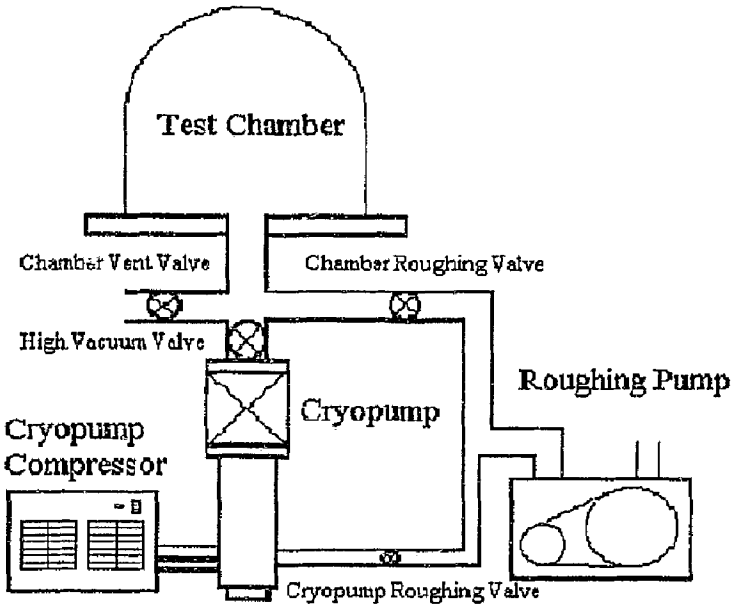


**Figure 18 - Schematic of the Vacuum Chamber[32]**

Compressed air was used to operate the various valves that were used to operate the vacuum chamber. The compressed air was regulated at approximately 70 psi which was supplied in the laboratory. From the schematic the main components of the vacuum chamber can be seen. The system consists of a roughing pump, cryopump, numerous valves, and a cryopump compressor. The cryopump compressor pumps helium into the head of the cryopump to reduce the temperature to about 10-20 degrees Kelvin.

### 4.1.1 Vacuum Chamber Pumps

There are two pumps that are used to operate the vacuum chamber. The first pump that is used is the rough pump which decreases the pressure in the chamber from atmospheric pressure to 100 milli torr. Once 100 milli torr is reached the cryopump is used which would further reduce the pressure to low as $1.5 \times 10^{-5}$ torr. The extremely low temperature

of the cryopump is able to condense the air in the vacuum chamber, which reduces the pressure. However, when gas is flowing into the chamber the pressure increases to 1-$3x10^{-4}$ torr depending on the flow rate. Since the pressure in the chamber stabilizes when there is gas flow into the chamber there is no time restriction on how long the chamber can effectively be used.

### 4.1.2 Bell Jar Hoist

Originally, when the vacuum chamber was first set up the only way the bell jar, which weighs approximately 100 pounds, could be raised and lowered was with a forklift[31]. This proved to be very inefficient and very time consuming. This process also required the presence of a laboratory technician. This problem was assigned as a senior project and the solution was to implement a hoist[33]. The hoist mechanism was attached to the side of the bell jar and a motor lowers or raises the bell jar with a push of a button. Both the lowering and raising option can be down at two speeds. The bell jar raised by the hoist can be seen in Figure 19.

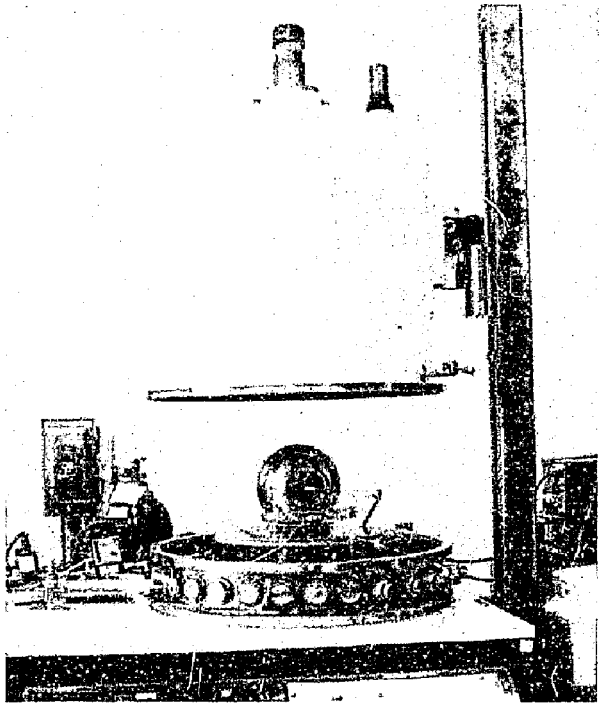

Figure 19 - Bell Jar and Hoist

## *4.2 Thruster Setup*

The thruster requires numerous power supplies and a source of fuel to operate it. The power supplies are used to supply power to the cathode to emit electrons and to the anode. Power supplies are also needed to supply a voltage to the grids and the Langmuir probe.

### 4.2.1 Power Supplies

The cathode (heater) supply was a Hewlett Packard 6263B DC power supply which can range from 0 volts to 24 volts and 0 amps to 12 amps and is shown in Figure 20. This power supply could provide enough current to the tungsten wire so that the needed

emission could be obtained. The heater (cathode) power supply was connected to the two threaded rods which hold the tungsten filament.

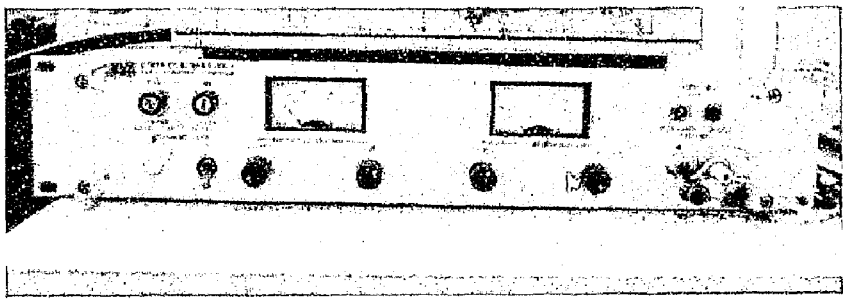

**Figure 20 – Heater (Cathode) Power Supply**

Since there was no beam extraction there was only one power supply for the grids instead of two, which would normally be used if a beam was extracted. The two grids, which were biased with the cathode common, were shorted and a GW GPR-30H10D DC power supply was used to provide the negative potential. The grid power supply is shown in Figure 21. The outputs of the grid power supply were digital which made recording data precise. One of the main readings for the discharge curves was the total current to the girds which was able to be read to the nearest thousandth of an amp. The grid power supply is capable of supplying 0 volts to 300 volts and 0 amps to 1 amp of current.

Figure 21 - Grid Power Supply

The anode potential was provided by a HP 6038A DC power supply, which was also biased with the cathode common. The positive end of the power supply was connected to the anode and the anode was biased with the cathode common. The anode power supply is shown in Figure 22.

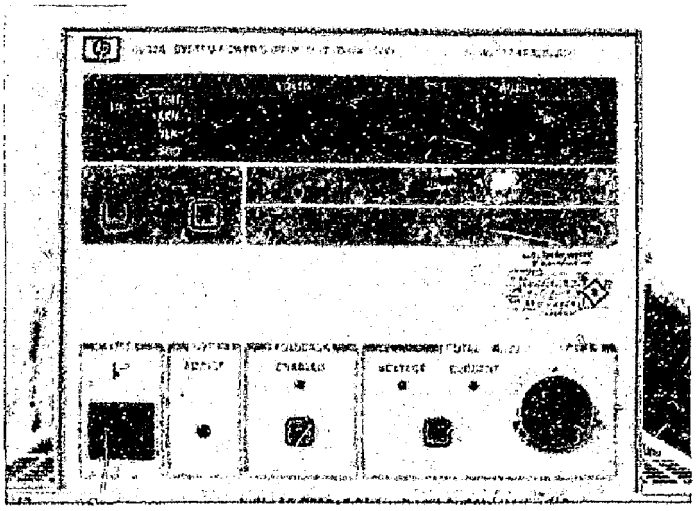

Figure 22 - Anode Power Supply

Similar to the gird power supply the readings from the anode power supply are important for the performance curve calculations. The readings are digital and offer enough accuracy with the discharge voltage being read to the nearest tenth of a volt and the

discharge current able to being read to the nearest hundredth of an amp. The anode power supply was capable of supplying 0 volts to 61.3 volts and 0 amps to 10 amps of current.

A KEPCO bipolar power supply that can be adjusted from -100 V to +100 V was used to apply a potential to the probe. The current collected by the probe was measured by placing a resistor in series with the circuit. Since the resistance value and the voltage value could be measured by a multimeter the current was easily calculated using Ohm's Law. Ohm's law is a relationship between voltage, current, and resistance where voltage is equal to the product of the resistance and current ( *voltage = current × resistance*). A wiring diagram consisting of all the power supplies and the connections to the probe, anode, and grids is shown in Figure 23.

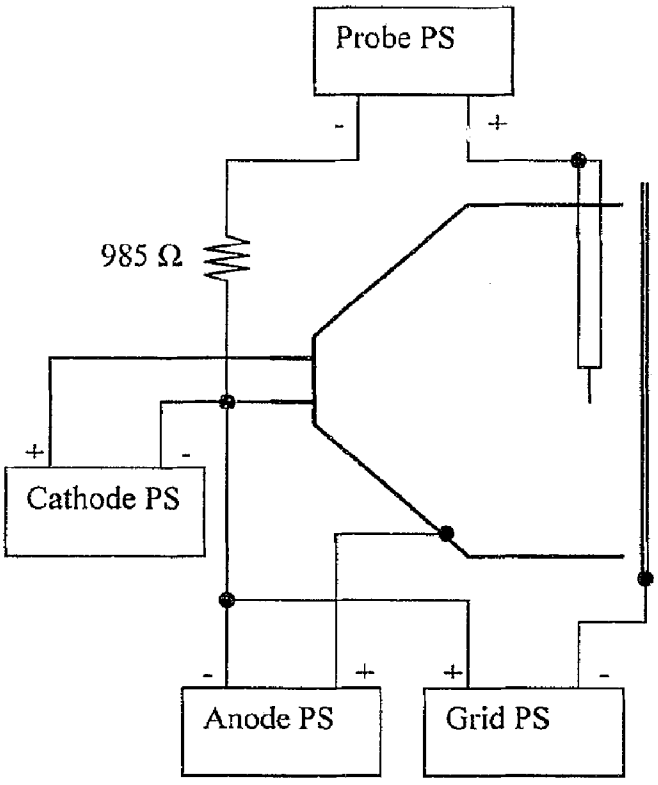


**Figure 23 - Wiring Schematic**

### 4.2.2 Fuel Supply

Argon gas, which is a noble gas, was used as fuel because it has very similar properties to xenon but costs much less. The argon was supplied in a tank with a flow regulator attached. The flow regulator on the tank did not control the flow to the thruster with any accuracy it was just used to let the gas out of the tank. Figure 24 shows the Aalborg flow meter that was used in this experiment to determine the flow rate. The flow meter was capable of measuring up to 20 sccm (standard cubic centimeter per minute).

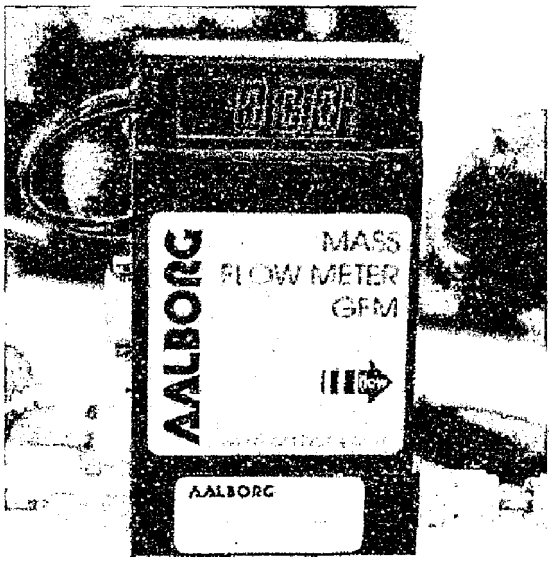


**Figure 24 - Aalborg Flow Meter**

The flow meter is calibrated with nitrogen, not argon or xenon, and the difference must be taken into account when calculations are made. To correct for a different gas a K factor is used which is derived from gas density and coefficient of specific heat. To convert from a flow rate displayed on the gage the K factor is multiplied by it. In Table 2 K factors are shown for the two gases that were used in this experiment.

**Table 2 - K Factors**

| Gas | K Factor |
|---|---|
| Argon | 1.4573 |
| Xenon | 1.44 |

The Aalborg flow meter was not capable of controlling the flow, only measuring it. As a result a needle valve was used to control the flow rate. The needle valve is shown in Figure 25.

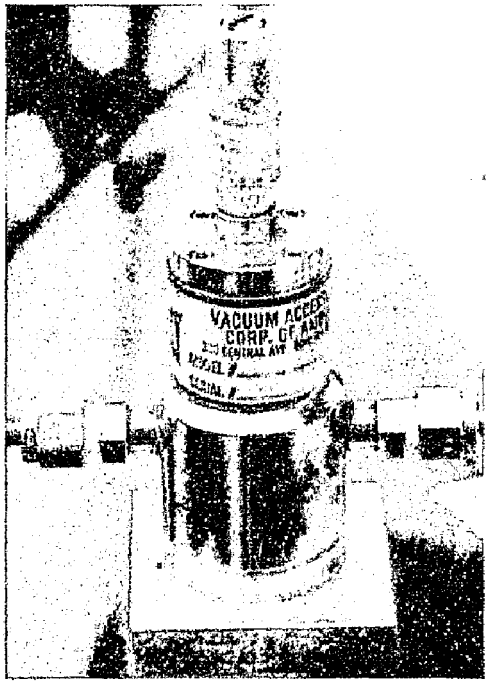

**Figure 25 - Needle Valve**

The needle value was adjusted manually and the flow meter was used to observe the flow rate. The fuel flow path is shown below in Figure 26.


**Figure 26 - Fuel Flow Path**

To verify if the Aalborg flow meter was displaying the correct value another flow meter was used. The other flow meter was a Teledyne Nall 100 which was donated by JPL. The two flow meters showed very similar readings and the Aalborg was used throughout the experiment because the Teledyne reading would often fluctuate between different numbers in the tenth of a sccm range.

### 4.2.3 Traverse

The traverse system was upgraded to a motorized system. The mechanically driven system had a device through one of the ports in the vacuum chamber and was manually adjusted from outside the vacuum chamber. The mechanically driven system proved to be insufficient for this project because the positional accuracy was low. Also it was not possible to accurately duplicate data without first pressurizing and opening the chamber and recalibrating the probe position. This proved to be very time consuming and the accuracy of the position was unreliable. A motorized traverse system was investigated to solve the problems with the mechanically driven system. Systems that were already assembled by various companies were found to be expensive with the prices being $1000-$2000. A less expensive solution was found by observing that an ink jet printer has a device very similar to a traverse system. A Canon Bubble Jet printer was taken apart and the track system was left intact. The printer track system consisted of a chassis, belt, and a stepper motor. The track system is shown in Figure 27. Stepper motors are widely used in precision applications, such as printers, and thus would fulfill the accuracy requirement needed for the probe traverse.

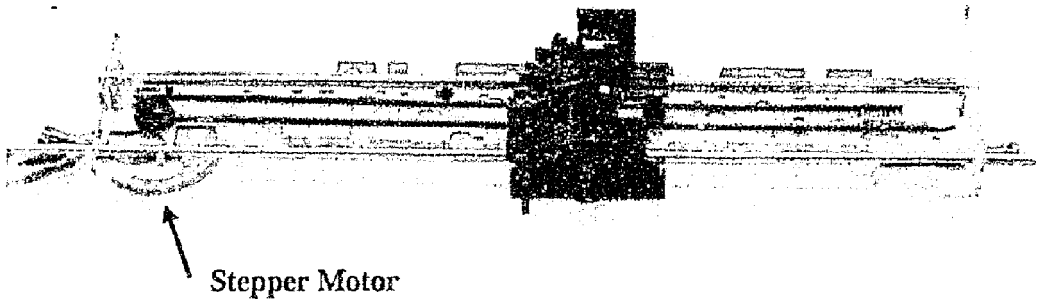


Figure 27 – Traverse Track System

To control the stepper motor a stepper motor controller and driver were needed. These items were obtained in a kit from All Motion. The stepper motor would be controllable by a PC with an RS485 converter which connects to the COM port on the PC. HyperTerminal, which was integrated with Lab View, was used to send the commands to the stepper motor. The probe traverse was moved with commands that were inputted into HyperTerminal/Lab View. For example the command "/1A523R" would be used to move the probe traverse to a position that would require 523 steps. One cm was found to be about 95 steps.

# CHAPTER 5: TESTING AND PROCEDURE

In this experiment five magnet geometries were tested, including the magnet geometry that the thruster was originally designed for. The magnet geometries changed the magnetic field inside the discharge chamber which includes changes to the maximum closed magnetic contour line of the thruster, the field lines that the electrons follow, and the plasma volume inside the discharge chamber. For each of the magnet geometries the cathode filament was positioned in four different locations axially. Both the magnet geometry and the cathode position should have on affect on the performance of the thruster and the beam profile.

After numerous initial tests it was found that the performance of the thruster was time sensitive. This is because the thruster performance changes as the temperature inside the discharge chamber changes as a result of the heat produced by the tungsten filament during operation. It is important to take this effect into account so that the data collected could be compared.

## *5.1 Magnet Geometries*

The five magnet geometries tested are shown in Figure 28. The unfilled blue rectangles are the original magnets and the solid red rectangles are magnets that were added. The north pole of the magnets is shown by the arrow in the figure and it can be seen that the polarity is alternating with each successive row of magnets for all magnet geometries.

Magnet Geometry 1

Magnet Geometry 2

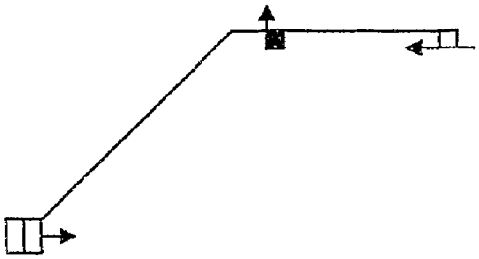

Magnet Geometry 3

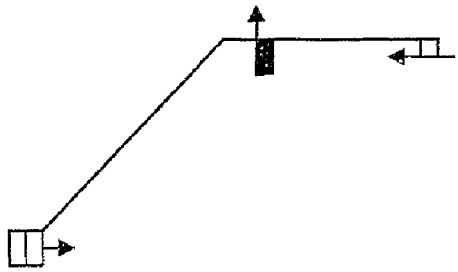

Magnet Geometry 4

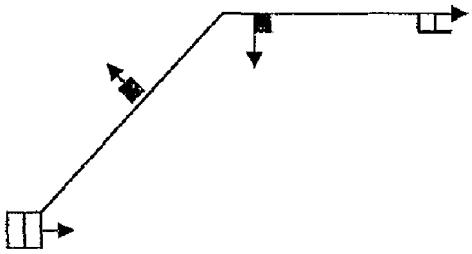

Magnet Geometry 5

**Figure 28 - Magnet Geometries**

Magnet geometry (MG) 1 is the geometry the thruster originally came with. It can be seen that there are two magnet rings, or ring cusps, one magnet ring near the cathode and the other magnet ring near the exit plane. MG 2 has is similar to MG 1 but the magnetic ring near the exit plane is strengthened. This will show if the performance of the thruster can be increased without the addition of another magnet ring to minimize the losses at the cusp. MG 3 is similar to MG 1 but adds another ring near the center of the thruster. MG 4 is the same in MG 3 but strengthens the middle magnetic ring and MG 5 will have four magnetic rings.

## *5.2 Filament Locations*

For all magnet geometries the position of the cathode was varied. The cathode filament was positioned at 1", 1.5", 2.5", and 3.4" from the cathode plate. The measurements are referenced to the cathode plate as shown in Figure 29.

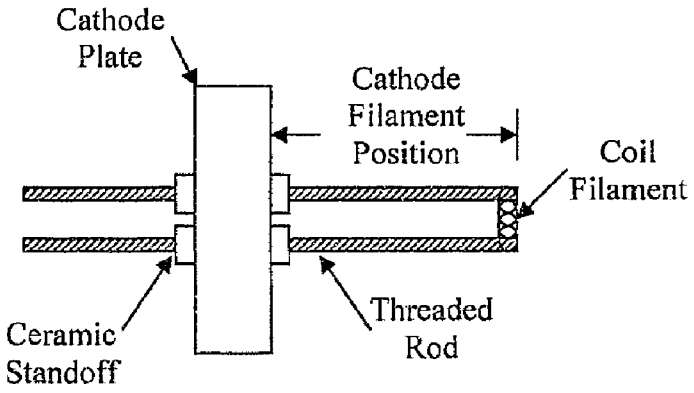


**Figure 29 - Measurement of Cathode Filament Position**

The cathode filament positions were chosen so that a broad range of locations could be observed with a higher concentration near the cathode plate.

Figure 30 shows the positions of the cathode filament with respect to the cross sectional view of the 15-cm thruster with a MG 1 configuration; the cathode filament locations looked identical for the other four magnet geometries.

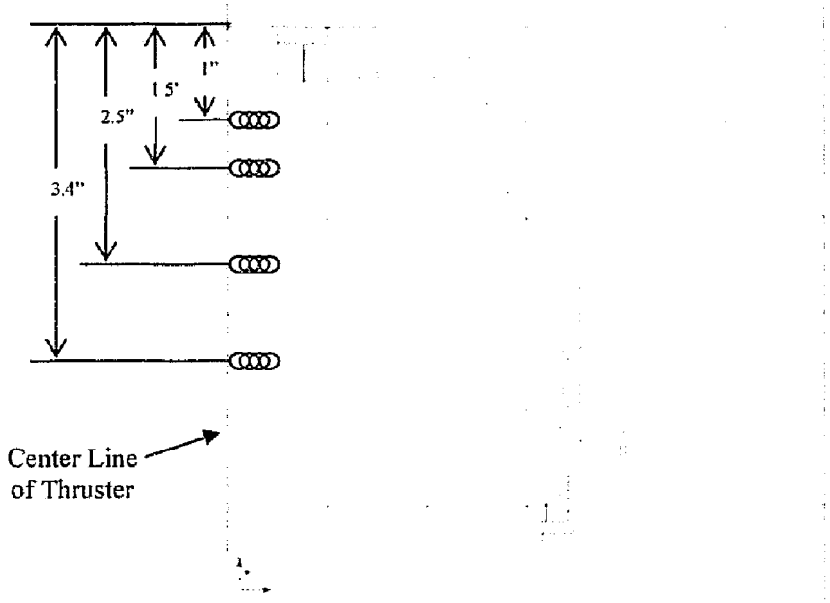


**Figure 30 - Cathode Filament Locations**

## *5.3 Beam Profile Measurements*

The beam profiles were obtained by a Langmuir probe which consisted of a 0.25" diameter circular tip made of stainless steel. The circular tip was held by a double bore alumina ceramic rod which had an outside diameter of 0.094". The ceramic material is

non conductive and can withstand the high temperatures in the discharge chamber. Figure 31 shows the probe attached to the traverse and a close up view of the probe tip.

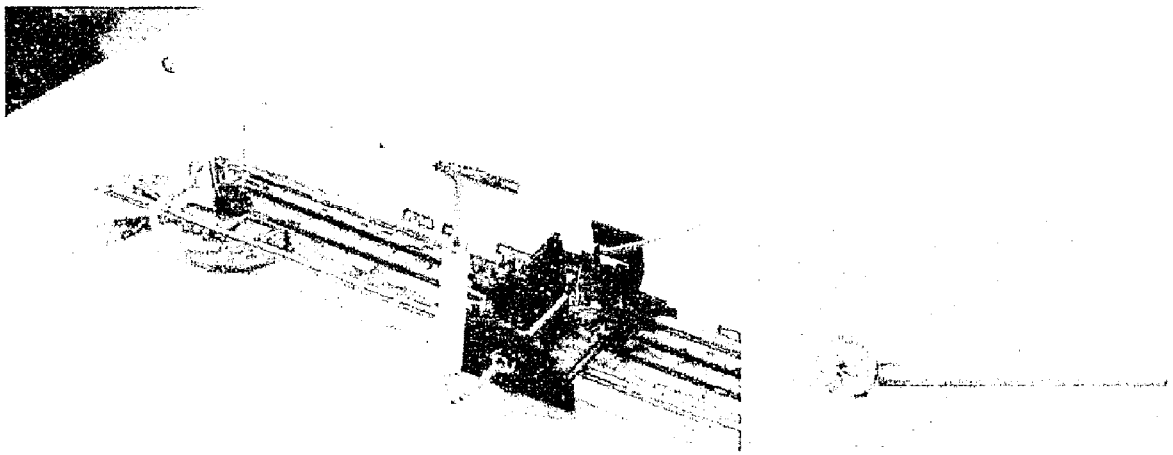

**Figure 31 - Probe attached to Traverse and Close-Up View of Probe Tip**

The probe was oriented to minimize the size of the opening necessary to insert the probe into the discharge chamber. In order to insert the probe into the thruster a small hole was made into the grid enclosure and a small slit was made in the thruster near the exit plane. Figure 32 shows the probe inserted into the discharge chamber upstream of the grids.

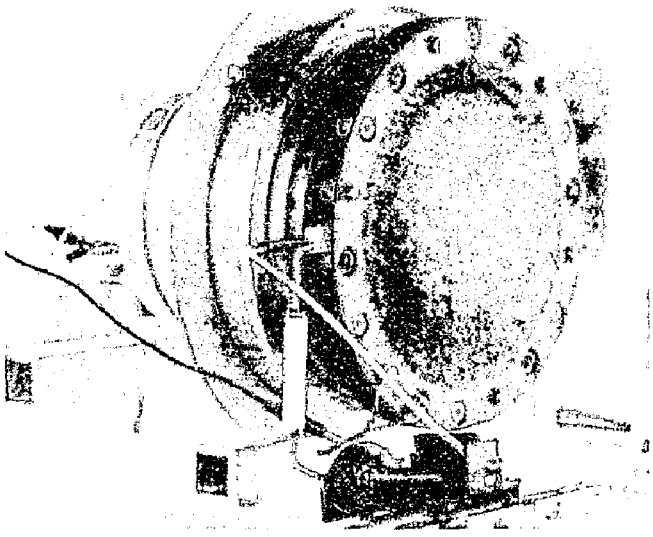

**Figure 32 - Probe Inserted Into Discharge Chamber**

The tip of the probe was located near the center of the thruster, as shown in Figure 32. The traverse, controlled using LabView, was used to move the tip of the probe from the center to the edge of the thruster. Measurements were made every centimeter starting from the center of the thruster to get acceptable resolution of the beam profile.

A test case was performed to ensure that the probe was accurately placed in the center of the exit plane. Figure 33 shows a beam profile for MG 4 at a filament location of 1.5". The figure shows that the 0 cm position has the highest current density and the current densities at -1 cm and 1 cm are similar which indicated that the probe was positioned correctly.

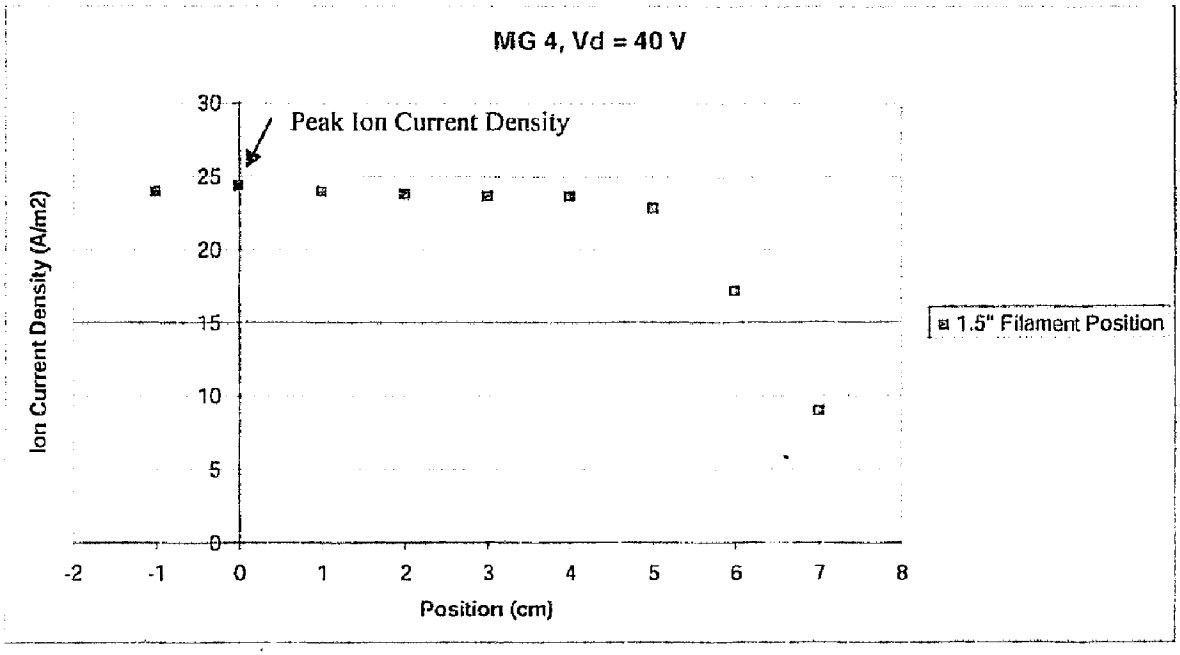


**Figure 33 - Center Probe Location Test**

## *5.4 Operational Thruster Parameters*

It was necessary that the operating conditions of the thruster remain identical for each test so that meaningful comparisons could be made with the collected data. The flow rate for all the tests was 4.0 sccm as read on the gage; however, as stated earlier, the K factor has to be taken into account. With the inclusion of the K factor the flow rate was 5.83 sccm. The anode voltage was set to 40 V for all five magnet geometries and for comparison purposes the anode voltage was set to 30 V for MG 2.

Ion thrusters have a higher performance with a larger discharge voltage; however the life of the thruster is reduced dramatically due to erosion. As a result there is a trade off between performance and the life of the thruster. The cathode (heater) voltage ranged from 6-10 V depending on the desired discharge current. The grid voltage was -40 V

biased with the cathode common to collect the ions in the discharge chamber. The voltage of the grids was based on when the ion current to the grids saturated as shown in Figure 34.

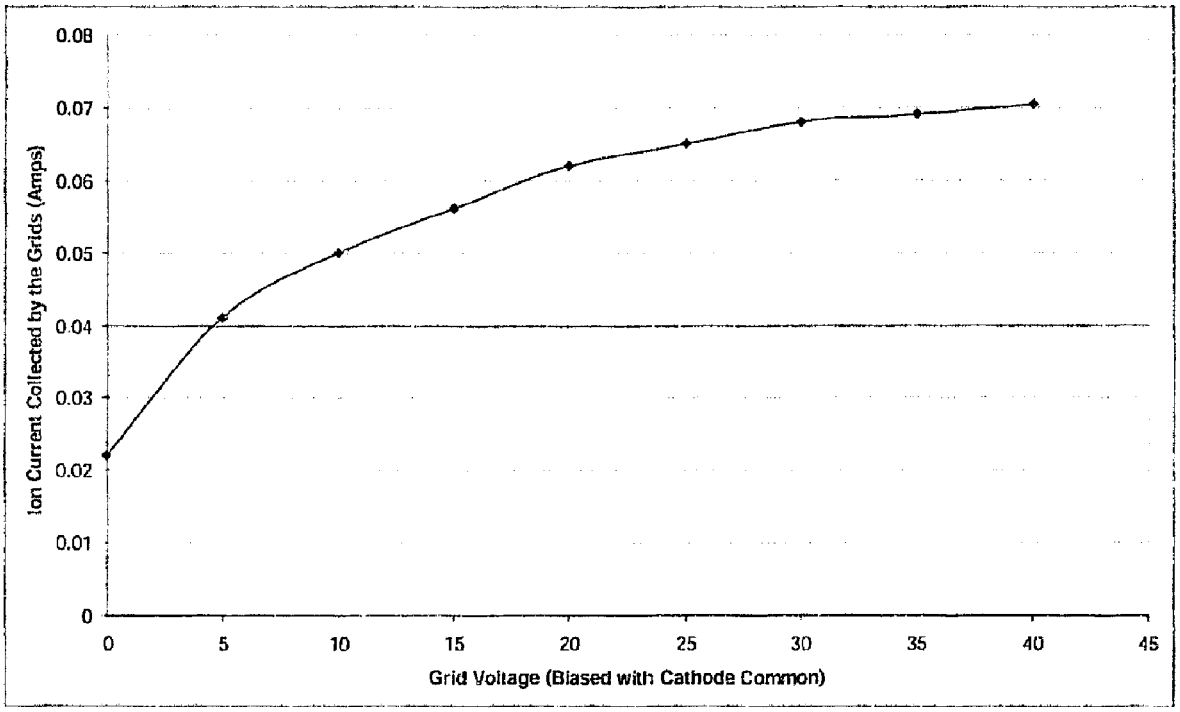


**Figure 34 - Grid Voltage Determination**

In Figure 34 it can be seen that the ion current to the grids reaches an asymptote and begins to level off around 35-40 volts, consequently a voltage of -40 V was chosen. Literature suggested that the probe voltage be at the same potential as the grids, in this case -40 V biased with the cathode common[31]. The cathode voltage and cathode current were varied for each desired discharge current and is further discussed in section 5.5. Table 3 summarizes the operating conditions of the thruster.

Table 3 - Thruster Operating Conditions

| | |
|---|---|
| Flow Rate (sccm) | 5.83 |
| Anode Voltage (V) | 40 |
| Grid Voltage (V) | -40 |
| Probe Voltage (V) | -40 |
| Cathode (Heater) (V) | 6-10 |
| Cathode (Heater) (A) | 4-8 |

All the voltages are biased with the cathode common.

## 5.5 Procedure

During each test the flow rate was first set to the desired value and then the anode and the grid power supplies were turned on. The cathode power supply was adjusted until the discharge current read 0.75 amps. At this point there was a 25 minute standby so that the transient effects of the thruster heating are diminished. Then the probe power supply was turned on before the beam profile measurements were taken. The beam profiles were taken between 25-30 minutes after the cathode power supply was first turned on. Beam profile measurements were taken at the center of the thruster to the edge of the thruster at 1 centimeter increments. Once the beam profile measurements were taken the probe tip was positioned near the edge of the thruster so that there was no interference of the ions to the grids. As stated earlier, the performance curves were obtained by keeping the flow rate and the discharge voltage constant while varying the discharge current which consequently changed the ion current to the grids. To obtain the performance curve the discharge current was set to 0.75, 1.25, 1.75, 2.25 and 2.75 amps. For each discharge current the ion current to the grids was measured with the grid power supply. At the 30 minute mark the ion current to the grids was measured when the discharge current was 0.75 amps. After each ion current to the grid measurement the discharge current was

increased by 0.5 and the ion current to the grids was measured at 2 minute intervals for each discharge current. Table 4 shows the timing sequence for each test.

**Table 4 - Timing Sequence**

| Time (minutes) | Task |
|---|---|
| 0-25 | Warm-Up |
| 25-30 | Beam Profile Measurements |
| 30 | Measurement of $\hat{J}_g$ at $I_d = 0.75$ amps |
| 32 | Measurement of $\hat{J}_g$ at $I_d = 1.25$amps |
| 34 | Measurement of $\hat{J}_g$ at $I_d = 1.75$ amps |
| 36 | Measurement of $\hat{J}_g$ at $I_d = 2.25$ amps |
| 38 | Measurement of $\hat{J}_g$ at $I_d = 2.75$ amps |

This timing sequence allowed for comparisons to be made with an assurance that the differences between all the cases were not the result of data being collected at different thruster conditions.

The discharge current, $I_d$, did not exceed 2.75 amps since a higher discharge current would prematurely burn out the tungsten filament. As a result of not using a higher discharge current there was a limit on the maximum mass utilization efficiency that could be attained.

# CHAPTER 6: RESULTS AND DISCUSSION

In this experiment a 15-cm ion thruster was tested and optimized. Experiments were conducted with simulated beam extraction and a tungsten filament used as the electron source. A total of five magnet geometries were tested including the original magnet geometry of the thruster. Performance of the ion thruster was quantified by calculating the performance curves and by obtaining the beam profile at the exit plane of the thruster with a Langmuir probe.

## *6.1 Magnet Geometry 1 Results*

MG 1 was the original magnet geometry designed for the 15-cm ion thruster. One magnet ring was located near the cathode with another ring near the exit plane of the thruster. A cross sectional view of the thruster is shown in Figure 35. In the figure the blue rectangles represent the samarium cobalt magnets. Figure 35 shows the maximum closed magnetic contour line to be about 22 gauss, which was obtained from Maxwell SV.

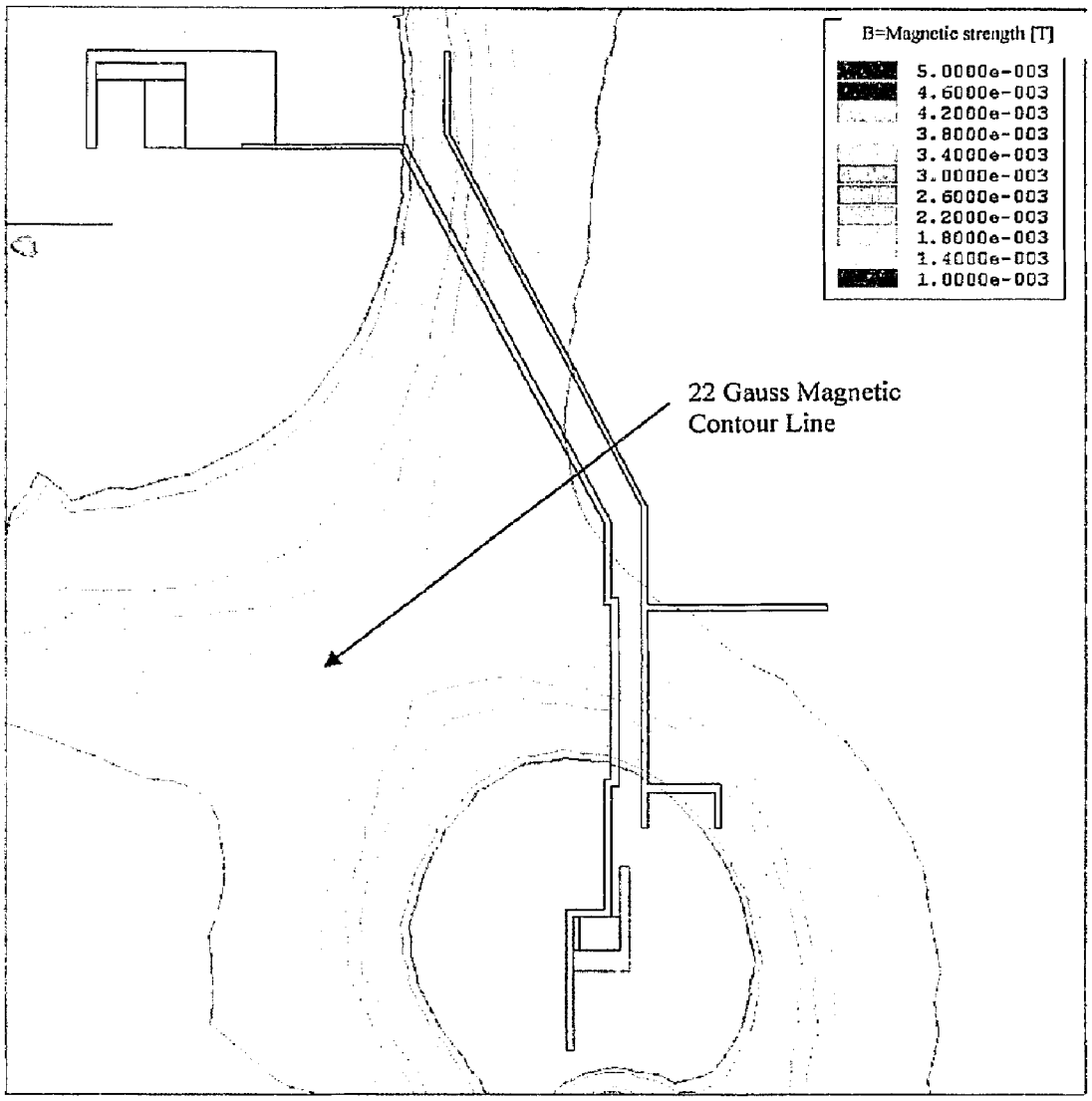


**Figure 35 – MG 1 Magnetic Field Plot**

MG 1 does not close the 50 gauss magnetic contour line so the plasma volume was found for the volume inside the last closed magnetic contour which was 22 gauss. The plasma volume was found to be 400 $cm^3$. The performance curves of MG 1 with the four different cathode filament positions are shown in Figure 36. A low value of the discharge loss is desirable since it represents the electrical cost of ionizing an atom. From Figure 36 it can be seen that the 1" position offers the worst performance while 1.5" offers the best

performance. The 2.5" position has a similar performance to the 1" position but the performance is worse. The 3.4" position is marginally higher performing than the 1" position but is worse than the 1.5" and 2.5" positions. As stated previously the discharge current was varied from .75 amps to 2.75 amps at 0.5 amp increments which is why each of the curves have 5 data points. With a discharge current 0.75 amps the mass utilization efficiency was about 32-35% and with a discharge current of 2.75 the mass utilization efficiency was about 68-72%.

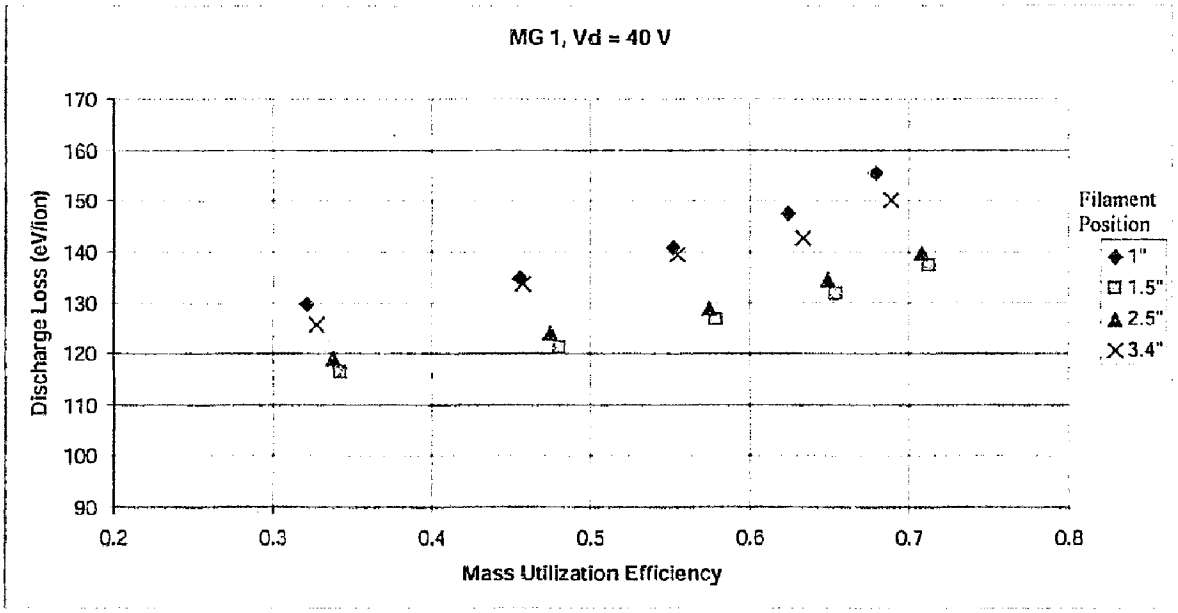


**Figure 36 - MG 1 Performance Curves**

It can be seen that the discharge loss increases as the mass utilization efficiency increases. This implies that in order to ionize more atoms more energy is required. It is also seen that the increase in the discharge loss is nearly exponential and that a great amount of energy would be needed to obtain mass utilization efficiencies near 100%. For

comparison of the different positions the discharge loss was found at a mass utilization efficiency of 65% and is shown in Table 5.

**Table 5 - Discharge Loss for MG 1 at 65%**

| Position | 1" | 1.5" | 2.5" | 3.4" |
|---|---|---|---|---|
| Discharge Loss (eV/ion) | 151 | 131 | 135 | 144 |

The discharge loss was found to be 131 eV/ion at the highest performing location of 1.5".

The beam profiles of MG 1 are shown in Figure 37 for the different cathode filament positions. Position 0 represents the center of the thruster and the ion current density at that location is about 26-27 A/m$^2$ for all positions.

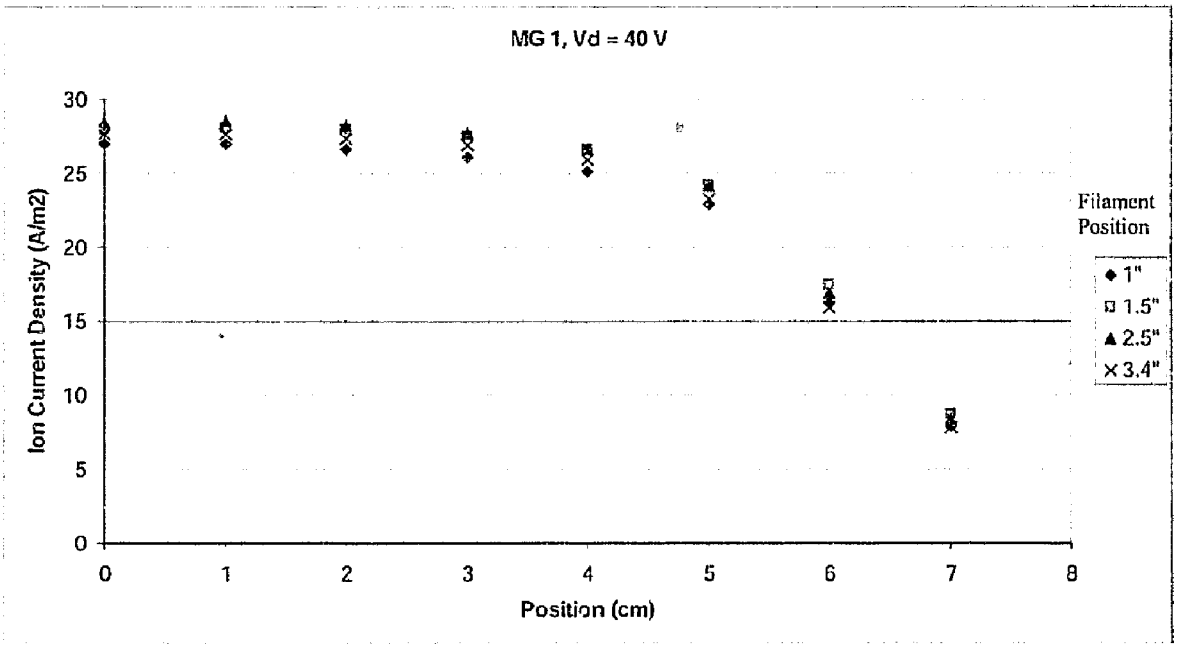


**Figure 37 - MG 1 Beam Profiles**

To verify if the ion current densities were correct the beam profiles were integrated to find the total ion current to the grids. From that calculation it was determined that the ion current densities were too high compared to the ion current that was measured from the grid power supply. This was the result of secondary electron emission which was caused by the ions hitting the surface of the stainless steel probe. As the ions strike the probe an additional electron was released causing the ion current to be measured higher than it actually was. The secondary electron emission does not have an effect on the beam profile shape as a result the beam profiles were corrected for by a factor. That factor was determined by comparing the integration of the beam profiles to the measured current by the grid power supply. A fifth order polynomial was fitted to all the beam profiles and was integrated. Equation 16 shows how the factor was calculated. The ion current to the grids, measured by the grid power supply, was divided by the calculated ion current to the grids. The ion current to the grids was calculated by the fifth order polynomial being integrated over the surface of the grids.

$$factor = \frac{\hat{J}_g}{2\pi \int_0^R r \bullet j_i(r) dr} \qquad \text{Equation 16}$$

In Equation 16 $\hat{J}_g$ is the ion current at the grids, r is the radial position, R is the radius of the grid, and $j_i(r)$ is the fifth order polynomial. A factor of 0.71 matched the integration of the beam profiles and the measured current by the grid power supply to within 1%. This factor was also applied to the other 4 magnet geometry beam profiles and also matched to within 1%. The corrected beam profiles are shown in Figure 38.

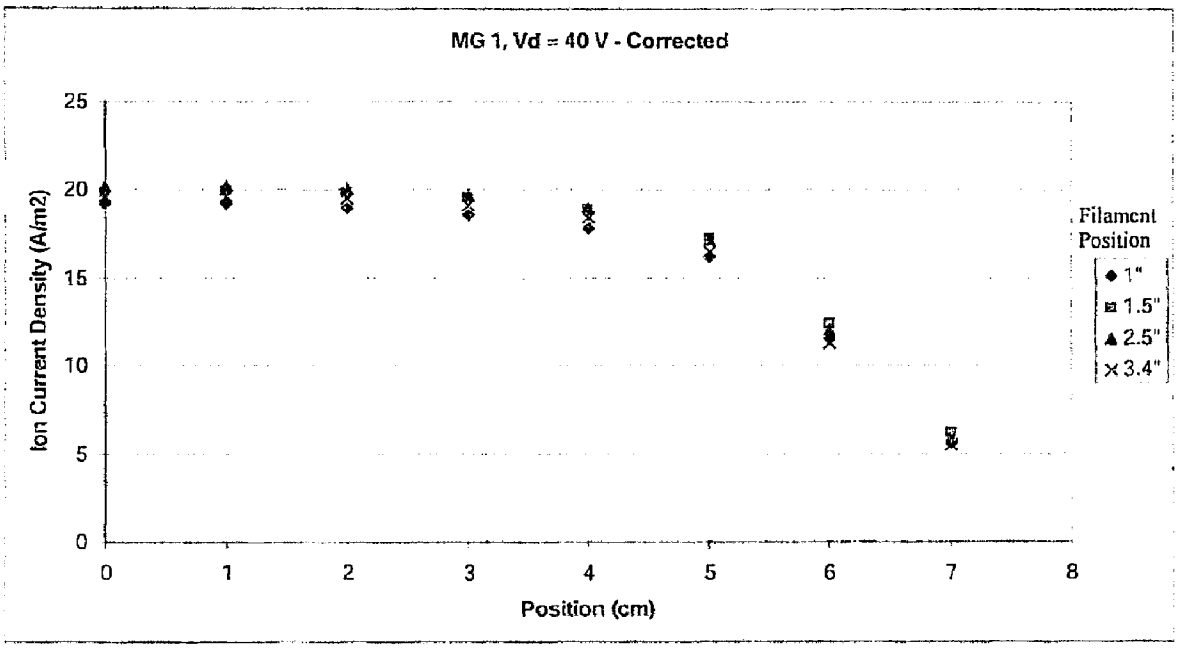


**Figure 38 - MG 1 Beam Profiles - Corrected**

The corrected beam profiles have the peak in the same location but the peak values are reduced to about 20 A/m$^2$. The beam profiles appear to be very similar in profile for all four positions and the values of the ion current densities are consistent with the performance curves. From Figure 36 it was found that the 1" position was the lowest performing position and from Figure 38 it can be seen that the 1" position has the smallest ion current densities.

From the center of the thruster to about 5 cm radially outward the beam profile is flat. After 5 cm from the axis of the thruster the ion current densities begin to decrease rapidly. Using Equation 11, the beam flatness parameter for the highest performance case, which was 1.5", was found to be 0.683. The beam flatness parameter will be compared with the other magnet geometries to show which geometry offers the best beam profile.

## 6.2 Magnet Geometry 2 Results

MG 2 is similar to MG 1 with the addition of a strengthened magnet ring near the exit. The magnet geometry and the magnetic field are shown in Figure 39 and it can be seen that the 28 gauss magnetic contour line is closed. This is an increase of about 6 gauss compared to MG 1.

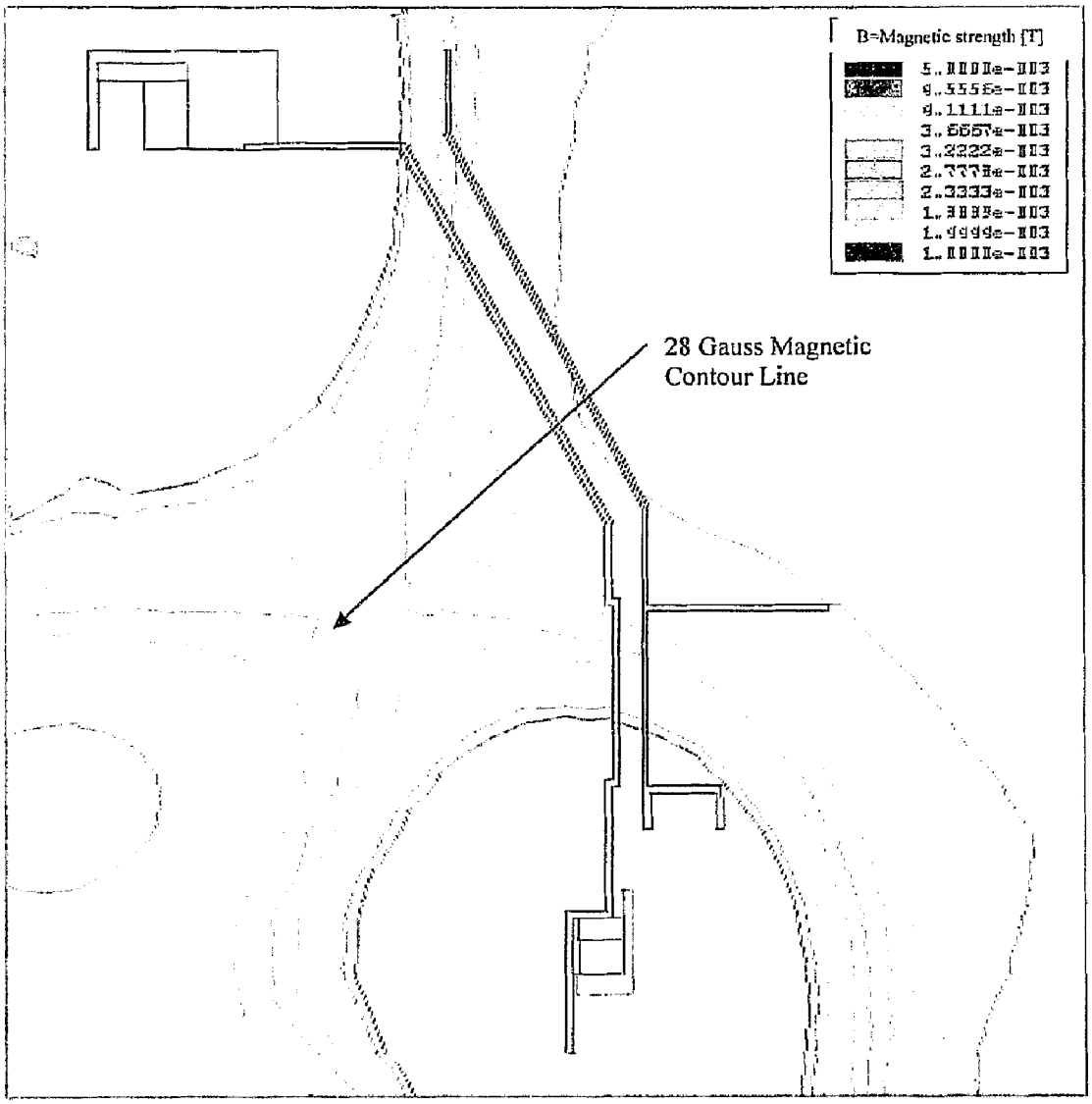


**Figure 39 - MG 2 Magnetic Field Plot**

Once again the 50 gauss magnetic contour line was not closed so the plasma volume was found for the volume inside the 28 gauss magnetic contour line (the last closed contour). The plasma volume was found to be 374 $cm^3$. Even though for MG 1 the 22 gauss magnetic contour line was used and for MG 2 the 28 gauss magnetic contour line was used, MG 2 was found to have a smaller plasma volume since the exit magnet ring was strengthened.

Figure 40 shows the performance curves for MG 2 for the different cathode filament positions.

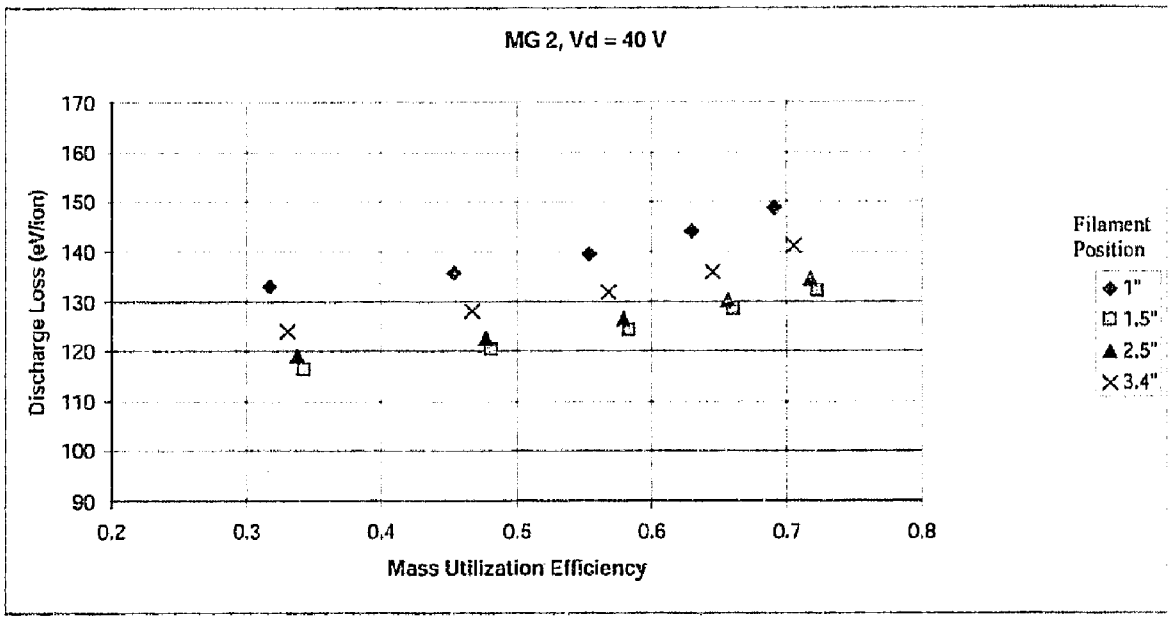


Figure 40 - MG 2 Performance Curves

The MG 2 performance curves were found to be similar to the MG 1 performance curves. The 1" position has the lowest performance while the 1.5" performance has the highest performance. The performance curves from positions 2.5" and 3.4" fall in the middle of

the two extremes. Table 6 shows the values of the discharge loss for MG 2 at a mass utilization efficiency of 65%.

**Table 6 - Discharge Loss for MG 2 at 65%**

| Position | 1" | 1.5" | 2.5" | 3.4" |
|---|---|---|---|---|
| Discharge Loss (eV/ion) | 145 | 128 | 130 | 136 |

At a mass utilization efficiency of 65% the discharge loss was found to be 128 eV/ion at a cathode filament position of 1.5". From the MG 1 and MG 2 performance curves it can be seen that MG 2 performs better than MG 1 which could be the result of the increased strength of the closed magnetic contour line.

Figure 41 shows the corrected beam profiles of MG 2. The beam profiles from the different positions have very similar trends with a peak in ion current density near the axis. Qualitatively the beam profiles from MG 2 do not seem as flat as the beam profiles from MG 1. There seems to be a constant decrease in the ion current density from the center of the thruster to about 4 cm. At about 4 cm the ion current density decreases rapidly.

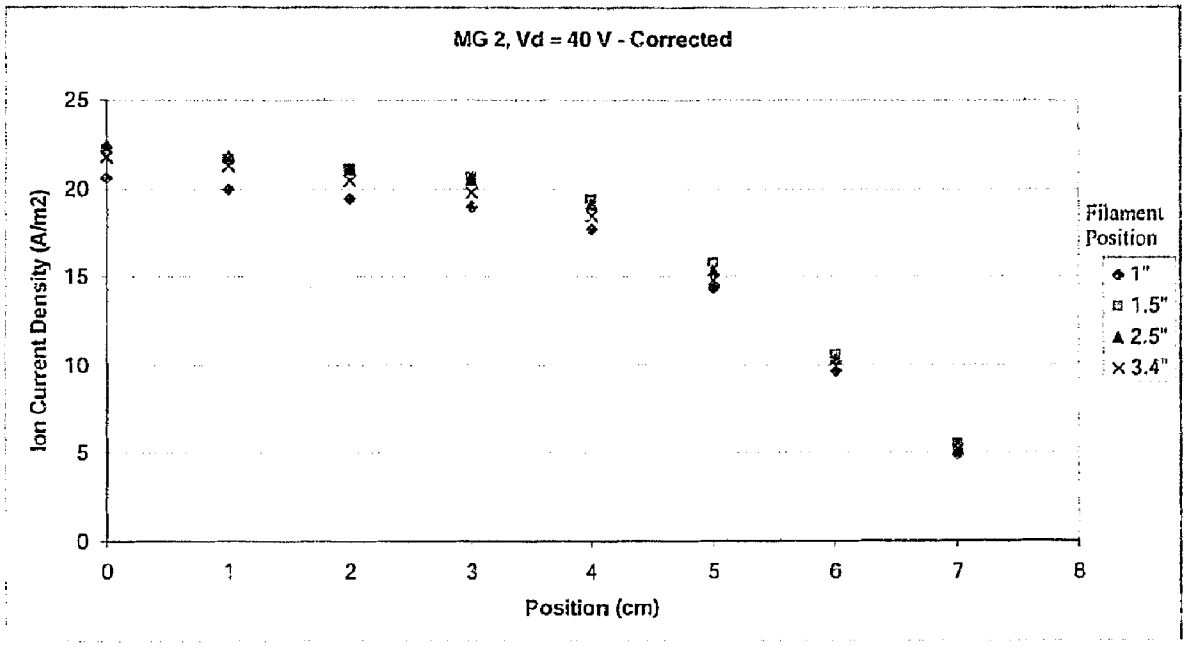


**Figure 41 - MG 2 Beam Profiles - Corrected**

As expected the 1" position beam profile has the smallest ion current densities because it was the lowest performing position. Also it can be seen that positions 1.5" and 2.5" have the largest current densities. For the 1.5" position the beam flatness parameter was found to be 0.613.

## *6.3 Magnet Geometry 3 Results*

MG 3 has three magnet rings where the third magnetic ring was placed near the center of the thruster about half way between the cathode and exit magnet rings. Figure 42 shows the magnetic field geometry of MG 3 and the closed 50 gauss magnetic contour line.

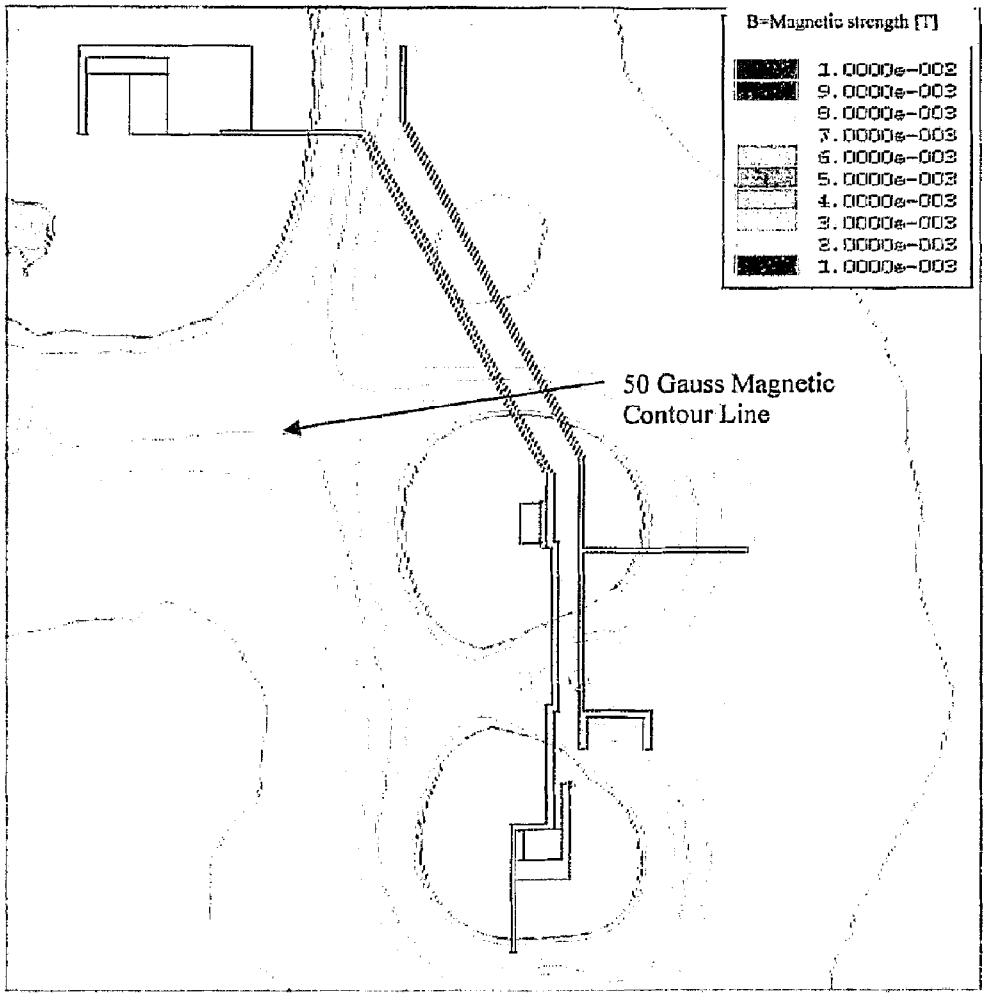


**Figure 42 - MG 3 Magnetic Field Plot**

The performance curves for MG 3 are shown in Figure 43. The plasma volume was found to be 843 $cm^3$ within the 50 gauss magnetic contour line. The main difference with the performance curves of MG 3 versus MG 1 and MG 2 is that the worst performance for MG 3 is from the 3.4" position instead of the 1" position. The 1.5" position still obtains the highest performance.

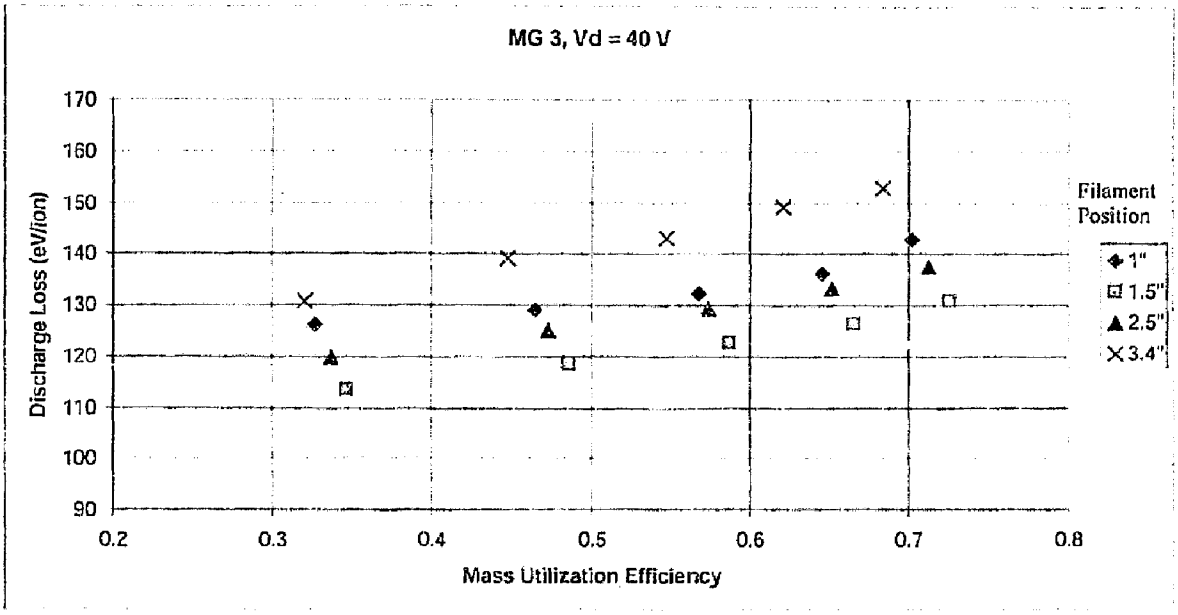


**Figure 43 - MG 3 Performance Curves**

The discharge loss for the 4 positions of MG 3 at a mass utilization efficiency of 65% is shown in Table 7. At the 1.5" position the discharge loss was 125 eV/ion, which is the most efficient thruster configuration from the three geometries thus far. MG 3 was found to be higher performing than MG 1 and MG 2 because of the 50 gauss magnetic contour line even though the plasma volume decreased for MG 3.

**Table 7 - Discharge Loss for MG 3 at 65%**

| Position | 1" | 1.5" | 2.5" | 3.4" |
|---|---|---|---|---|
| Discharge Loss (eV/ion) | 136 | 125 | 133 | 151 |

The 1.5" position is significantly better than the 3.4" position which had a discharge loss of 151 eV/ion. The beam profiles for MG 3 are shown in Figure 44. As with MG 1 and MG 2 the profiles seem relatively consistent for all of the different positions. The profiles appear to be very flat with a peak off axis at about 3 cm from the center.

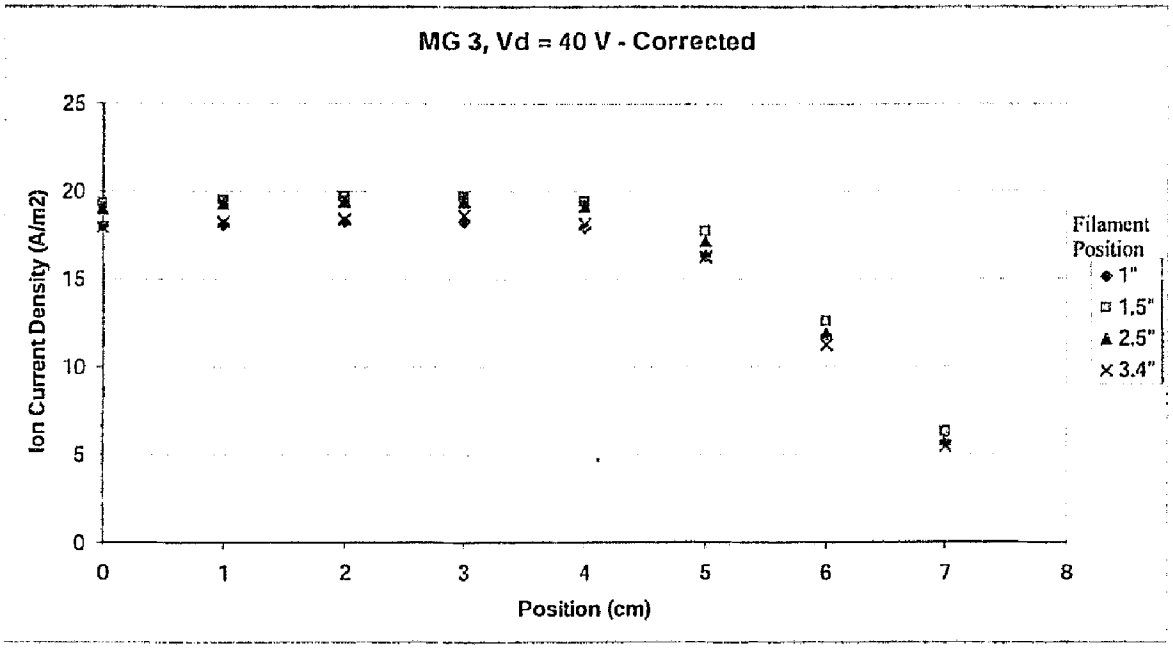


Figure 44 - MG 3 Beam Profiles - Corrected

The beam profiles begin to decrease significantly after 5 cm from the thruster axis. MG 3 had a beam flatness parameter of 0.705 at the 1.5" position.

## *6.4 Magnet Geometry 4 Results*

MG 4 attempts to do the same thing as MG 2, which was to increase the strength of the closed magnetic contour line but without adding another cusp. In MG 4 the middle magnet ring was strengthened by adding additional magnets which can be seen in Figure 45.

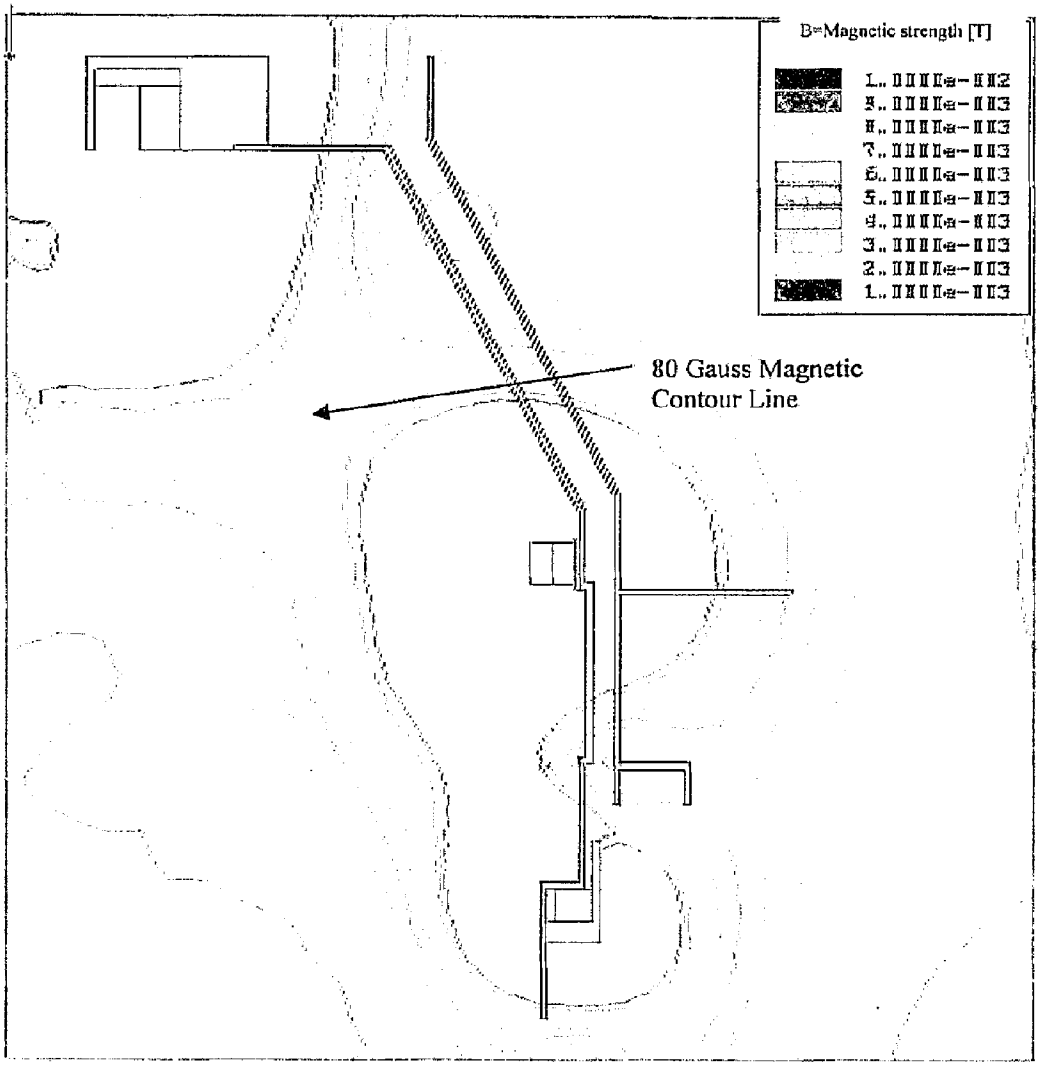


**Figure 45 - MG 4 Magnetic Field Plot**

From the Maxwell SV output it can be seen that the value of the closed magnetic contour line was increased compared to MG 3. From Figure 45 it is shown that the 80 gauss magnetic contour line closed the thruster. MG 4 has about a 30 gauss increase compared to MG 3. However, because the middle ring was strengthened, the plasma volume inside the discharge chamber was reduced. The plasma volume for MG 4 was 635 $cm^3$ within the 50 gauss magnetic contour line, a significant decrease from MG 3.

The performance curves for MG 4 are shown in Figure 46. Once again the data indicates that the 1.5" position offers the best performance. The worst performance was found to be when the filament was placed at 3.4".

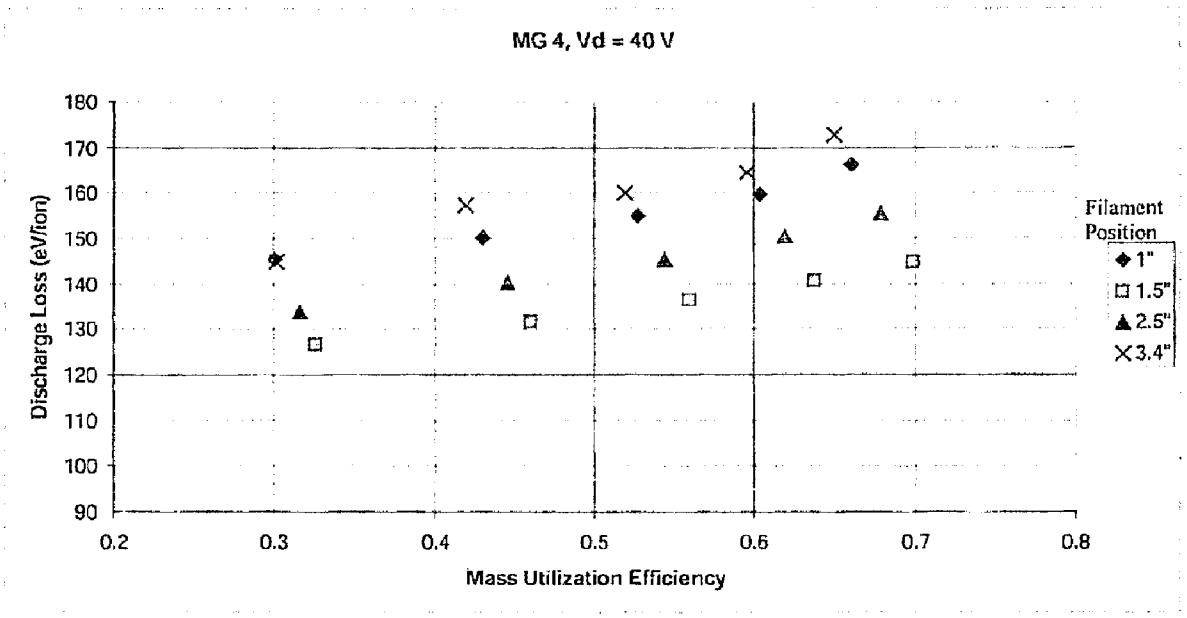


**Figure 46 - MG 4 Performance Curves**

The 2.5" position has a lower performance than the 1.5" position but was higher performing than the 1" position. In Table 8 the discharge loss for the different positions is shown at a mass utilization efficiency of 65%. Comparing MG 3 and MG 4 it can be seen that MG 4 is lower performing. The increase in the strength of the closed magnetic contour line to 80 gauss proves to be insufficient to overcome the loss in the plasma volume due to the strengthened middle magnet ring.

**Table 8 - Discharge Loss for MG 4 at 65%**

| Position | 1" | 1.5" | 2.5" | 3.4" |
|---|---|---|---|---|
| Discharge Loss (eV/ion) | 165 | 141 | 153 | 173 |

At a position of 1.5" the discharge loss was 141 eV/ion while at the lowest performing position the discharge loss was 173 eV/ion. The beam profiles for MG 4 are shown in Figure 47 and they show that there is small peaks near the axis but remain extremely flat to about 5 cm from the axis. Like most of the other geometries the ion current density reduces dramatically after 5 cm from the axis.

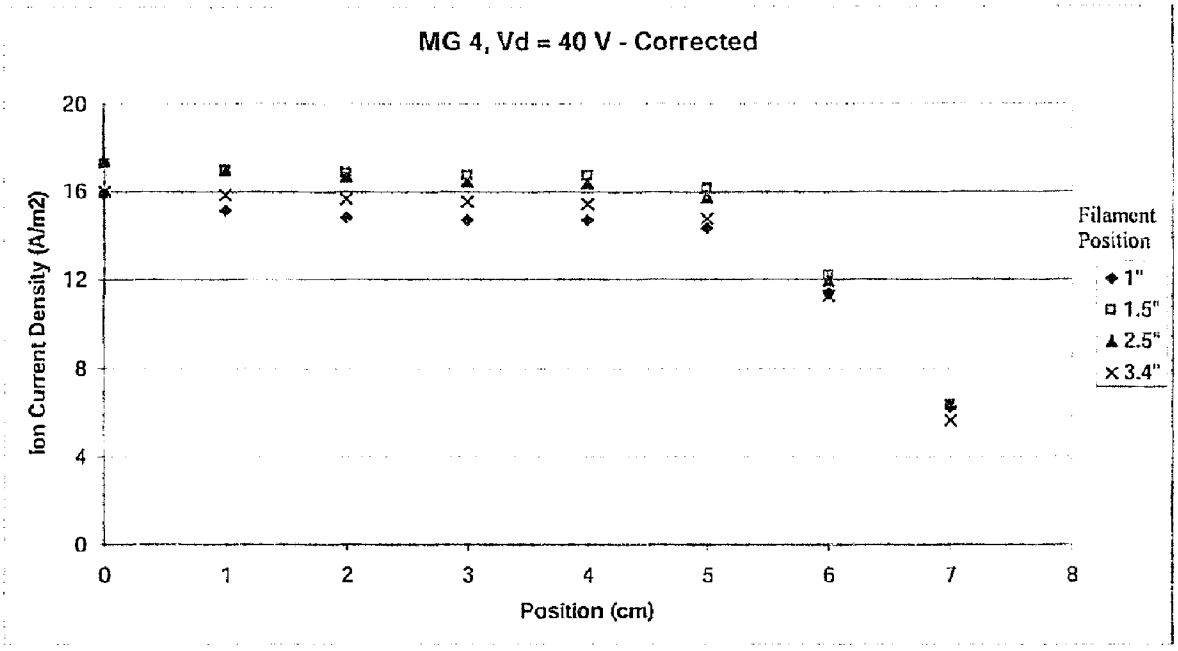


**Figure 47 - MG 4 Beam Profiles - Corrected**

All the beam profiles of the different positions have similar shapes and their differences in magnitude can be attributed to their performance. It was stated earlier that the 3.4" position performed the worst but it has larger ion current densities than the 1" position from 0 cm to about 6 cm; however from 6 to 7 cm the 1" position has a larger ion current density than the 3.4" position. Since a great deal of the area of the girds is location from 6

to 7 cm the 1" position results in capturing a larger ion current. For the 1.5" position the beam flatness parameter was 0.738.

## *6.5 Magnet Geometry 5 Results*

The last magnet geometry that was tested was MG 5 and was the only configuration that used 4 magnet rings. The cathode and exit plane rings were in the same locations and the magnet ring that was located near the conical section was place outside the discharge chamber while the magnet ring that was located near the cylindrical section was placed inside the discharge chamber. The geometrical setup of the 4 ring geometry is shown in Figure 48.

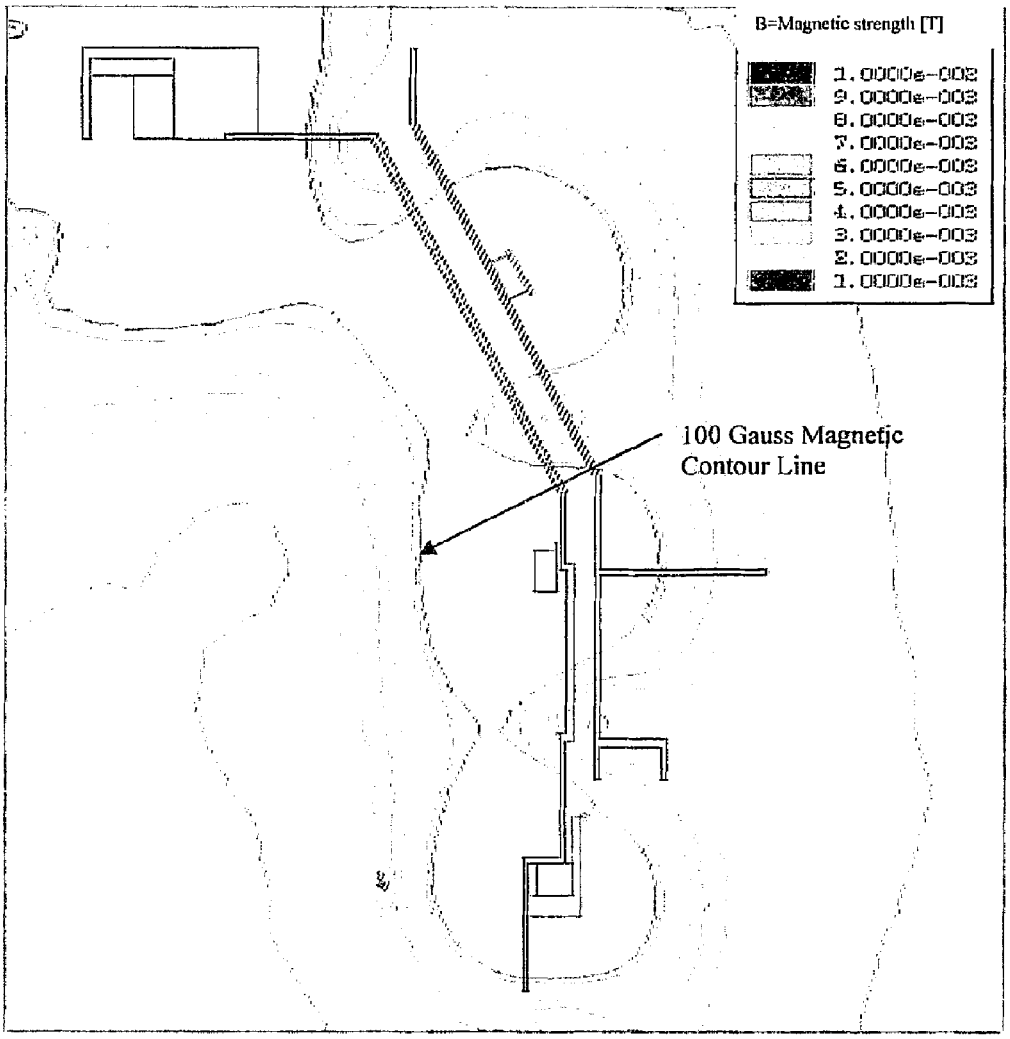


**Figure 48 - MG 5 Magnetic Field Plot**

The Maxwell SV output shows that the thruster closed the 100 gauss magnetic contour line and at the same time the magnetic free volume inside the discharge chamber increased because the magnetic contour lines were pulled closer to the anode wall. The plasma volume for MG 5 was 934 $cm^3$. However, there was a negative aspect to the 4 ring geometry which was that the additional magnet ring increased the losses because of the additional cusp.

The performance curves for MG 5 are shown in Figure 49. Position 1.5" remains the highest performing location but there is significant improvement for the 1" position compared to the other magnet geometries.

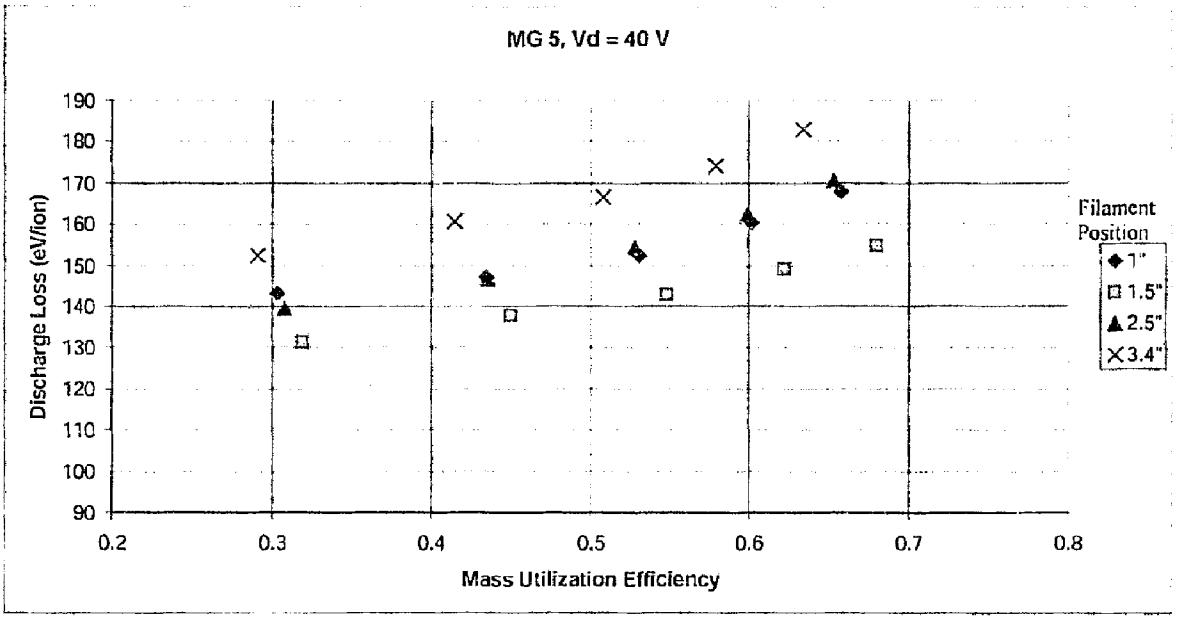


**Figure 49 - MG 5 Performance Curves**

There is a crossover in the performance curves for the 1" and 2.5" positions. The 2.5" position starts out being more efficient but at a mass utilization efficiency of about 47% the 1" position becomes more efficient. Table 9 shows the discharge loss for the different positions at mass utilization efficiency of 65%.

**Table 9 - Discharge Loss for MG 5 at 65%**

| Position | 1" | 1.5" | 2.5" | 3.4" |
|---|---|---|---|---|
| Discharge Loss (eV/ion) | 167 | 151 | 170 | 186 |

As with the other magnet geometries position 1.5" has the best performance with a discharge loss of 151.

Beam profiles for MG 5 are shown in Figure 50. The beam profiles are similar to MG 4 but do not have the small peak in the center. The profiles are extremely flat near the center and have the usual dramatic drop in ion current density near 5 cm from the center of the thruster.

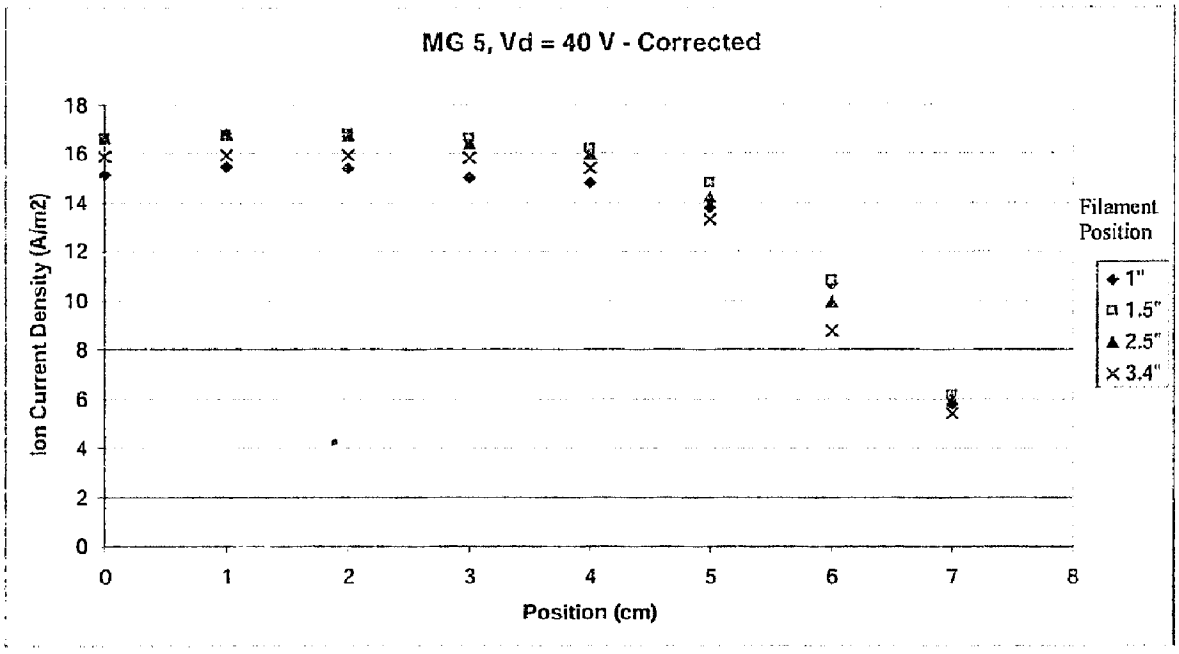


**Figure 50 - MG 5 Beam Profiles**

It can be seen that the 1" position has the lowest ion current densities up to about 4.5 cm and decrease at a slower rate than the other positions. As stated for MG 4, since a great deal of the area is located further from the center a small increase in ion current density could result in a significant increase in the ion current to the grids. As a result the 1"

position captures a larger amount of ions. For the 1.5" position the beam flatness parameter was found to be 0.739.

## 6.6 Comparison of Magnet Geometries and Discussion

To compare the different magnet geometries side by side the best performance curve from each magnet geometry was chosen. It was found that the best performance for all magnet geometries occurred at a filament location of 1.5". Figure 51 shows the highest performing curve from each of the magnet geometries.

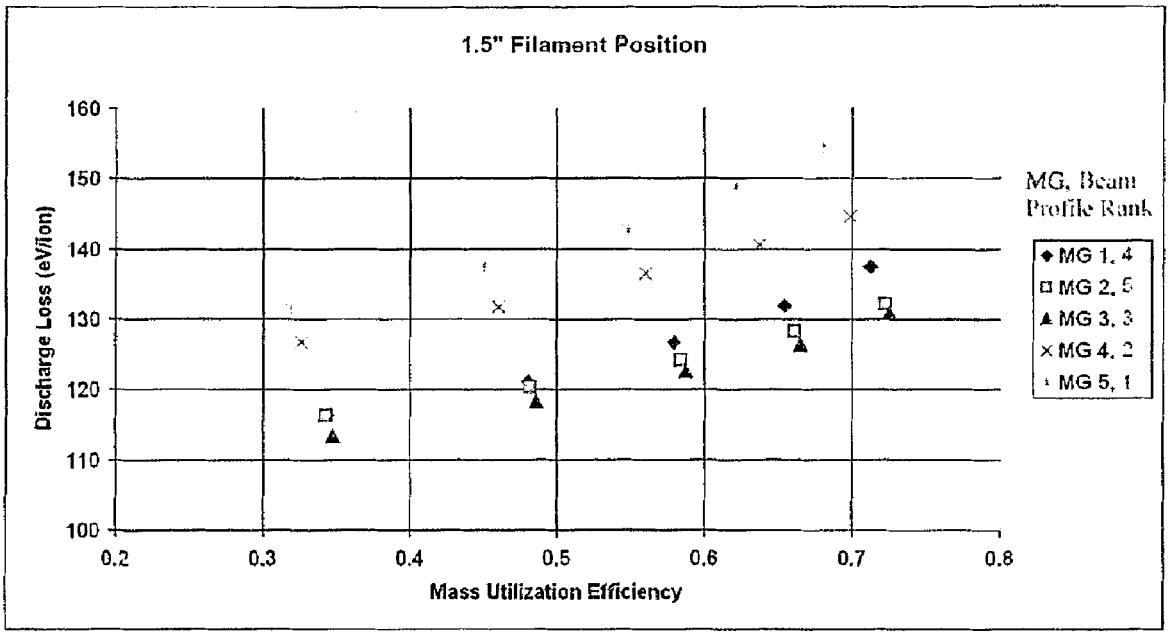


**Figure 51 - Highest Performing Curve from Each Magnet Geometry**

From Figure 51 it can be seen that MG 3, the three ring geometry, performed the best and MG 5, the four ring geometry performed the worst. The original magnet geometry, MG 1, performed worse than MG 2 and MG 3 but performed better than MG 4 and MG 5. The

performance is not simply based on the closed magnetic contour line but also the plasma volume inside the discharge chamber.

The corresponding beam profiles for the performance curves in Figure 51 are shown in Figure 52. The beam profiles are all fairly similar and are all relatively flat. This is in part because a filament cathode was used rather than a hollow cathode. A filament cathode artificially creates a flatter beam profile because of the way the electrons are emitted.

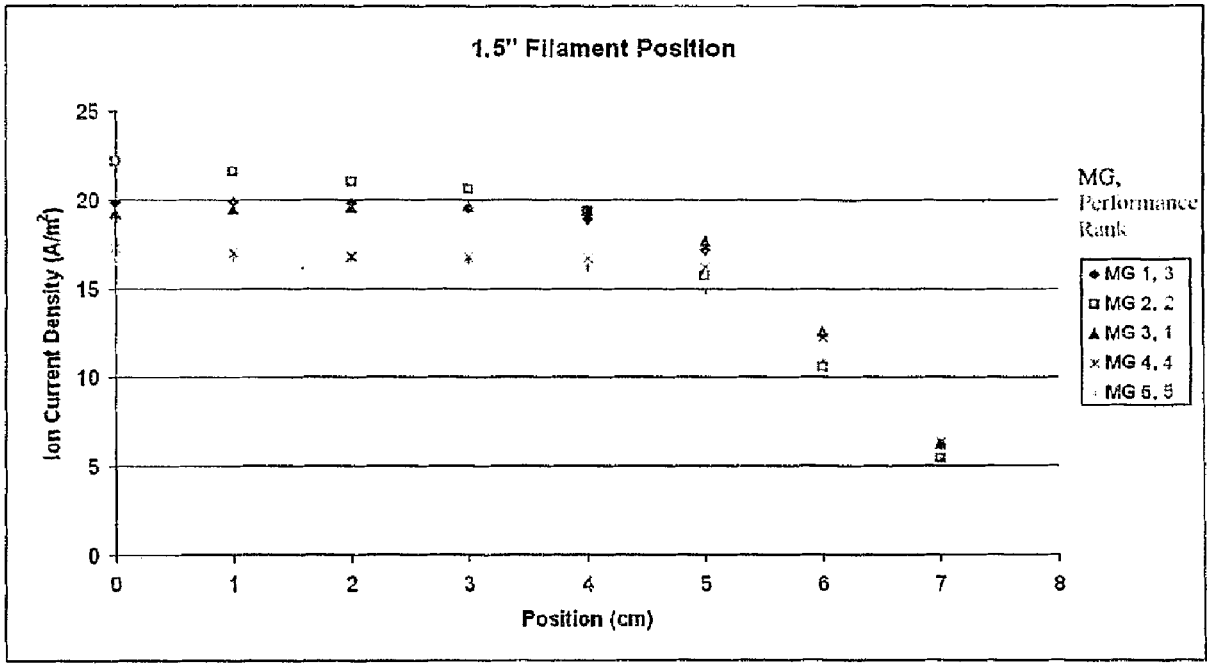


**Figure 52 - Highest Performing Beam Profile for Each Magnet Geometry**

Qualitatively comparing the beam profiles it is clear that MG 4 and MG 5 have the flattest beams, unfortunately they are also the lowest performing. MG 2 offers good performance but the beam profile is significantly uneven compared to the other beam profiles.

The performance of the different magnet geometries was found to be best at a filament position of 1.5". Figure 53 shows the axial magnetic strength for the MG 3 magnet geometry and why the 1.5" position was the best performing. From the figure it can be seen that at the 1.5" location there is a local maximum in the magnetic strength. At the 1.5" position the emitted electrons that are traveling towards the grids experience a favorable magnetic gradient; however, at the 1" position the emitted electrons experience an adverse magnetic gradient.

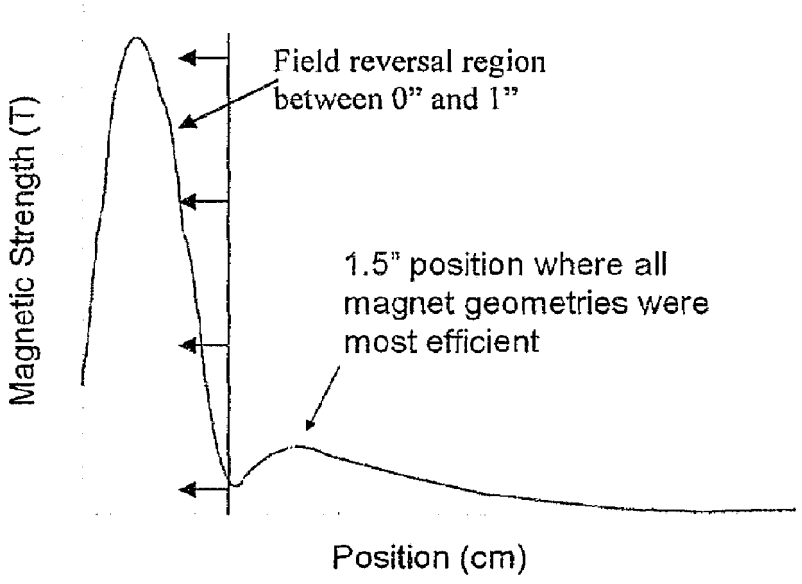


**Figure 53 - MG 3 Axial Magnetic Strength**

Between 0" and 1" there is a field reversal region due to the cathode magnet ring and if the filament were to be placed in that position the emitted electrons would be guided to the cathode plate instead of the discharge chamber. From the figure it could be concluded that the filament should be placed near the second maximum on the downhill side so the emitted electrons experience a favorable magnetic gradient for an optimum filament

location. The axial magnetic strength plots for the other magnet geometries are shown in Appendix A.

A summary of the results, including the $A_p$, V, and the $l_e$, for the 1.5" position for each magnet geometry is shown in Table 10. The electron path length, $l_e$, was not found for MG 1 and MG2 because the plasma volumes do not correspond to the closure of the 50 gauss magnetic contour line. The plasma volume for MG 1 and MG 2 should not be compared to the other magnet geometries for the same reason.

**Table 10 - Summary of Results**

| | $\eta_d$ (eV/ion) at 65% $\eta_m$ | Closed Magnetic Contour Line (gauss) | $f_p$ | $A_p$ ($cm^2$) | V ($cm^3$) | $l_e$ (cm) | Performance Rank | Beam Profile Rank |
|---|---|---|---|---|---|---|---|---|
| MG 1 | 131 | 22 | 0.683 | 2.42 | 400 | - | 3 | 4 |
| MG 2 | 128 | 28 | 0.613 | 1.29 | 374 | - | 2 | 5 |
| MG 3 | 125 | 50 | 0.705 | 3.32 | 843 | 254 | 1 | 3 |
| MG 4 | 141 | 80 | 0.738 | 3.07 | 635 | 207 | 4 | 2 |
| MG 5 | 151 | 100 | 0.739 | 7.21 | 934 | 129 | 5 | 1 |

From Table 10 it can be seen that the magnet geometry has an impact on the performance of the thruster. The two ranking columns rank the performance and the beam profile (1=best and 5=worst). The magnet geometry can influence the efficiency of the thruster and the flatness of the beam profile. The original magnet geometry, MG 1, seems to not have closed a sufficient magnetic contour line because the performance was increased simply by strengthening the exit ring. Although strengthening the exit magnet ring caused the plasma volume inside the thruster to decrease, the increase in the strength of the closed magnetic contour line caused the performance to increase. However, strengthening the exit ring also caused the beam profile to be the worst of all the magnet geometries.

With MG 3 another magnet ring was added to the ion thruster to pull the magnetic contour lines closer to the anode wall and to increase the strength of the closed magnetic contour line. The closed magnetic contour line strength was increased to 50 gauss. Unfortunately, the addition of the third magnetic ring also increased the loss at the cusp. It was found that increasing the closed magnetic contour line to 50 gauss and pulling the magnetic contour lines closer to the anode wall increased the performance even though losses at the cusp were increased. MG 4 attempted to do the same thing MG 2 did which was to increase the closed magnetic contour line strength without adding an additional cusp. With MG 2 the increase in the strength of the closed magnetic contour line caused the thruster to perform better despite the plasma volume being decreased because of the strengthened exit ring. However with MG 4 the increase of the closed magnetic contour line from 50 gauss to 80 gauss was not sufficient to overcome the decrease in the plasma volume because of the strengthened middle magnet ring. As a result the performance curves showed poor performance compared to MG 2 and MG 3. In order to increase the plasma volume a fourth ring was added for MG 5. MG 5 had a closed magnetic contour line of 100 gauss and the magnetic contour lines were closer to the anode wall. However the performance was extremely poor because of the losses at the cusp to due the additional magnet ring.

From Table 10 it can be seen that $A_p$ decreased for MG 2 compared to MG 1 and $A_p$ decreased for MG 4 compared to MG 3. The decrease in $A_p$ for MG 2 and MG 4 was because the magnet rings were strengthened and as shown in Equation 7, $A_p$ is a function of the magnetic strength. For MG 5, $A_p$ was much greater than the other magnet

geometries; this was the result of an additional ring but also because the fourth magnet ring was much further from the anode surface than the other magnet rings. The distance between the magnet ring and the anode surface caused the magnetic strength at anode surface to be much smaller resulting in larger $A_p$ because of the relationship shown in Equation 7.

The electron path length was calculated for three magnet geometries as shown in Table 10. The largest electron path length, 254 cm, corresponded to the highest performing configuration, MG 3. The smallest path length corresponded to the lowest performing configuration, MG 5, suggesting that the electron path length is a good measure of performance.

The values in Table 10 are shown in Figure 54 for a graphical comparison of discharge loss, closed magnetic contour line, and $A_p$.

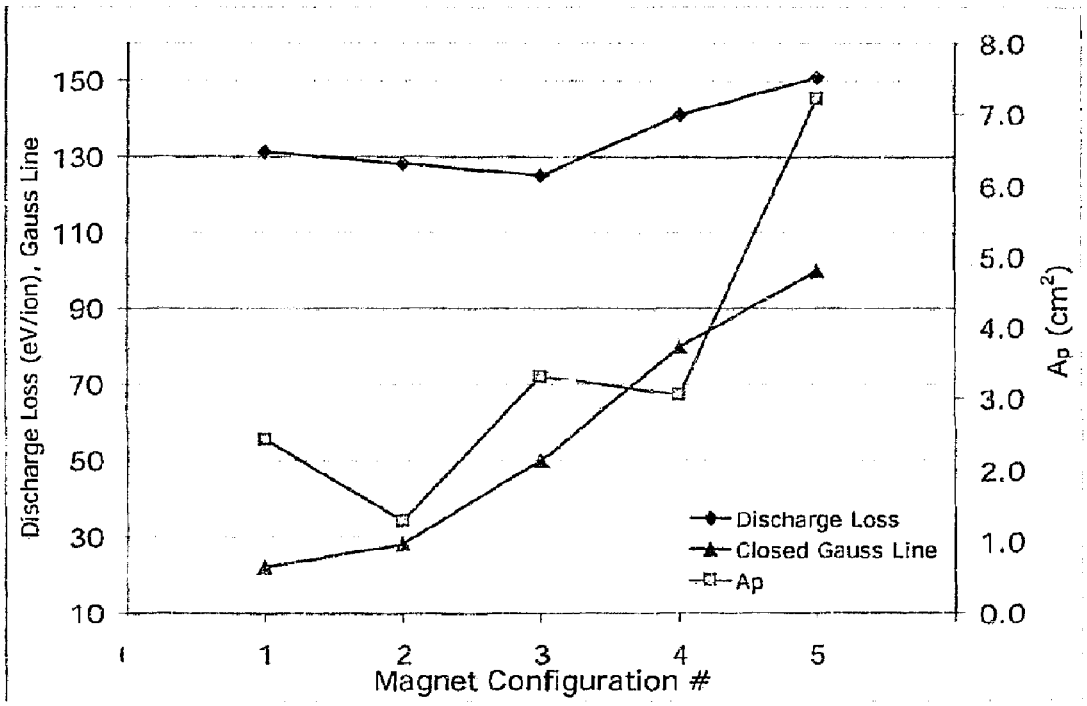


**Figure 54 - Performance Comparison**

The graph shows that the maximum closed contour has a positive effect up to a certain point and that $A_p$ has a dominating effect on MG 5.

Since most ion thruster are run at a discharge voltage close to 30 V a comparison was done to see the difference between a discharge voltage of 30 V and 40 V. Figure 55 shows that the performance of the ion thruster increased as the discharge voltage was increased.

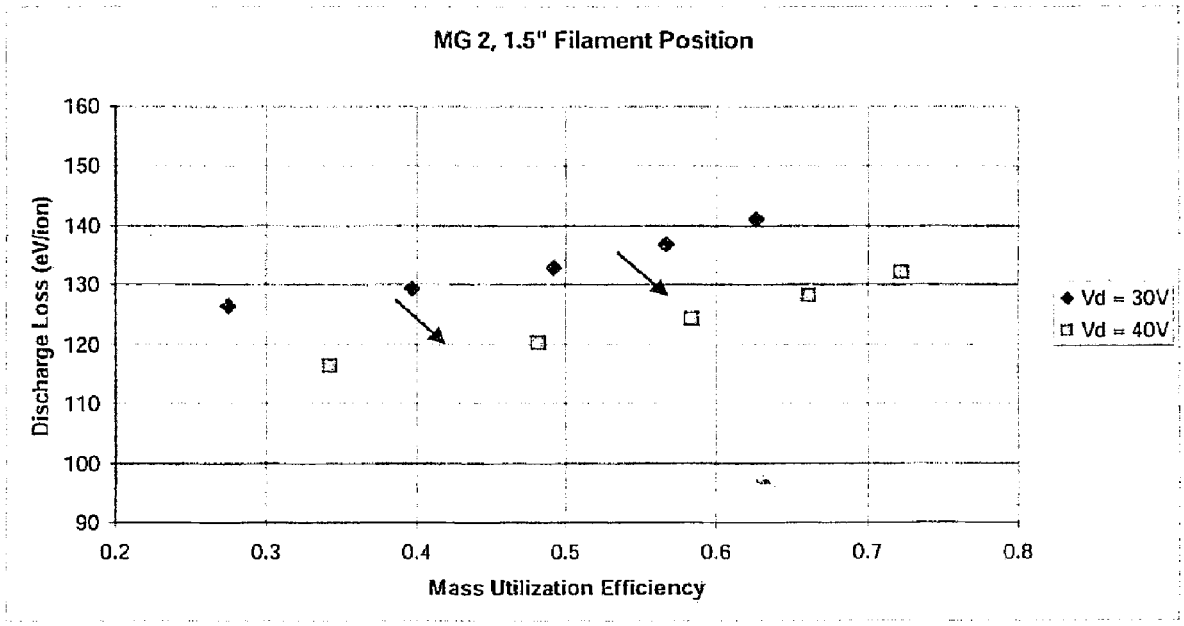


**Figure 55 - Comparison of MG 2 with Vd of 30 V and 40 V**

Although the performance of the ion thruster increases with increased discharge voltage the life of the thruster would be reduced because of the increased rate of erosion.

A test was also conducted using Xenon to see if there was an effect on the beam profile. The comparison is shown in Figure 56.

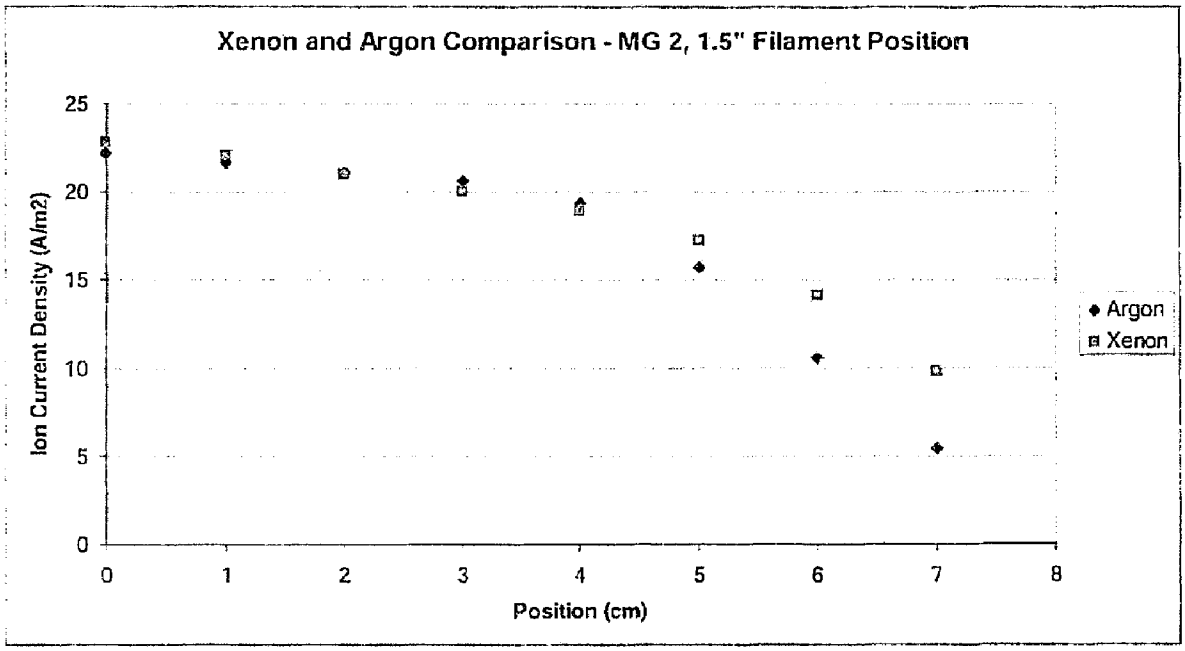


**Figure 56 - Comparison of Xenon and Argon for MG 2**

Near the center of the thruster to about 4 cm the ion current densities are similar. At the edge of the thruster the Xenon maintains larger ion current densities than the Argon. The beam flatness parameter was calculated to be 0.682 for the Xenon versus 0.613 for Argon. Using Equation 7 and substituting the ion masses for the electron mass it can be seen that a larger mass would have a larger Larmor radius. A Xenon atom has an atomic mass of 131.3 amu and Argon has an atomic mass of 39.9 amu. A larger Larmor radius allows the heavier Xenon atoms to penetrate the stronger magnetic field near the edge of thruster.

# CHAPTER 7: CONCLUSION

In these experiments, a 15-cm ion thruster was optimized with simulated beam extraction to produce the best beam profile at the lowest discharge loss. The objective of this thesis was to study ways to improve the performance of the 15 cm ion thruster. It was found that the performance of the thruster could be increased by varying two major components of the thruster, which consists of the cathode location and the magnet geometry. A total of five magnet geometries were tested, each with four different cathode positions. The magnetic field geometry was analyzed by using Maxwell SV, which is a magnetic and electrostatic-field solver. The axial movement of the cathode filament showed at what location the maximum amount of ions could be produced. Also, the magnet geometry was found to alter the beam profile at the exit plane of the thruster where the grids are located. Beam profiles were obtained by a Langmuir probe that was inserted just upstream of the grids in the discharge chamber. The Langmuir probe obtained readings from multiple positions with a computer controlled traverse mechanism. The ion thruster was tested with simulated beam extraction which allowed optimization of the discharge chamber without the high power consumption necessary for the acceleration of the ions. Simulated beam extraction also required less propellant flow which saved propellant and allowed for testing to be done in a smaller vacuum chamber because the background pressure did not increase as much as with beam extraction.

Performance was optimized by both changing the cathode filament position and by changing the magnet geometry. For all magnet geometries, the maximum performance

was attained when the cathode filament was at a location of 1.5". It was found that the original magnet geometry, MG 1, was not the best performing. MG 2 showed that a small increase in the closed magnetic contour increased the performance. The discharge loss decreased for MG 2 to 128 eV/ion from 131 eV/ion for MG 1 for a mass utilization efficiency of 65%. The highest performance was attained by the three ring geometry, MG 3, which had a discharge loss of 125 eV/ion. The strengthened three ring geometry, MG 4, performed much worse than the first three magnet geometries. MG 4 had a discharge loss of 141 eV/ion but attained a much flatter beam profile of 0.738. The four ring geometry, MG 5, had the worst discharge performance with a discharge loss of 151 eV/ion, but offered the flattest beam profile with a beam flatness parameter of 0.739. There was a tradeoff between the performance of the thruster and the beam profile; typically a higher performing configuration resulted in a lower beam flatness parameter. It was also found that the electron path length should be maximized to increase the ionization. In general, it was found that it would be desirable to have the largest possible closed magnetic field contour in the thruster while minimizing the number of magnet rings and at the same time maximizing the plasma volume inside the discharge chamber.

From the experiment it was found that performance does not always increase with increasing the strength of the maximum closed magnetic contour in the thruster. There were other factors such as the primary electron loss area, plasma volume, and the electron path length that had an influence on the performance. As the number of magnet rings was increased from 3 to 4 rings, there was a large increase in the primary electron loss area which reduced the ionization efficiency. To decrease the primary electron loss area, the

magnet rings could be strengthened in the 4 ring geometry, but this was not attempted. The electron path length for magnetic configurations MG 3 – MG 5 was calculated and it was found that as the electron path length decreased, so did the performance. Since the electron path length is a function of the plasma volume and the primary electron loss area, it is important to increase the plasma volume but at the same time decrease the primary electron loss area. Of the tested geometries, the three ring geometry performed the best in terms of discharge loss because it closed a sufficient magnetic field contour line, had a large enough plasma volume, and had the longest electron path length. However, the four ring geometry performed the best in terms of the beam profile, but requires stronger magnets to improve the primary electron confinement sufficiently to offset the larger magnetic cusp length and produce a low discharge loss.

For future work, it is recommended that use of a hollow cathode be included in the ion thruster testing. Previous attempts have been made but were unsuccessful. This was thought to be the result of the hollow cathode being contaminated during operation because the base pressure of the vacuum chamber was not low enough. However, there might be a chance that the argon which was used at the time was not pure enough. Two types of grids were donated by JPL and one type was used in this experiment. It would be interesting to test the other type and compare the data. Lastly, with some maturity of the program it would also be desirable to actually extract a beam by applying high voltages to the grids. While conducting future tests it would be advantageous predict the performance or implement a model to plan tests. A model has been developed at JPL by Dan Goebel which predicts the performance of a thruster by various inputs that do not

require the thruster to be operational[24]. The model should be used as a tool to plan and analyze further experimental testing.

# References


1. Goebel, D. M., Katz, Ira, Ziemer, J., Brophy, J. R., Polk, J. E., Johnson, L., "Electric Propulsion Research and Development at JPL," AIAA Paper No. 2005-3535, *41st Joint Propulsion Conference and Exhibit*, Tucson, Arizona, July 10-13, 2005.

2. Sengupta, A., "Experimental Investigation of Discharge Plasma Magnetic Confinement in an NSTAR Ion Thruster," AIAA Paper No. 2005-4069 (2005).

3. Herman, D. A., and Gallimore, A. D., "Near Discharge Cathode Assembly Plasma Potential Measurements in a 30-cm NSTAR-type Ion Engine amidst Beam Extraction," AIAA Paper No. 2004-3958 (2004).

4. Goebel, D. M., Brophy, J. R., Polk, J. E., Katz, Ira, and Anderson, J., "Variable Specific Impulse High Power Ion Thruster," AIAA Paper No. 2005-4246, *41st Joint Propulsion Conference & Exhibit*, Tucson, Arizona, July 10-13, 2005.

5. Herman, D. A., and Gallimore, A. D., "Discharge Chamber Plasma Structure of a 40-cm NEXT-type Ion Engine," AIAA Paper No. 2005-4250, *41st Joint Propulsion Conference and Exhibit*, Tucson, Arizona, July 10-13, 2005.

6. Brophy, J. R., "Simulated Ion Thruster Operation Without Beam Extraction," AIAA 90-2655, 21st International Electric Propulsion Conference, Orlando, FL, 1990.

7. Sutton, George P., and Oscar Biblarz. Rocket Propulsion Elements. New York: John Wiley & Sons, 2001.

8. http://www.boeing.com/defense-space/space/bss/factsheets/xips/xips.html

9. Beatrie, John R. "XIPS Keeps Satellites on Track," *American Institute of Physics* (1998): 24-26.

10. http://www.boeing.com/defense-space/space/bss/factsheets/xips/nstar/ionengine.html

11. Sengupta, A., Brophy, J. R., Goodfellow, K. D., "Status of The Extended Life Test of The Deep Space 1 Flight Space Ion Engine After 30,352 hours of Operation," AIAA Paper No. 2003-4558, *39th Joint Propulsion Conference and Exhibit*, Huntsville, Alabama, July 20-23, 2003.

12. http://nmp-techval-reports.jpl.nasa.gov/DS1/DS1_Results.pdf

13. http://nssdc.gsfc.nasa.gov/database/MasterCatalog?sc=1998-061A

14. http://www.grc.nasa.gov/WWW/ion/past/90s/nstar.htm

15. Brophy, J. R., Brinza, D. E., Polk, J. E., Henry, M. D., and Sengupta, A., "The DS1 Hyper-Extended Mission," AIAA Paper No. 2002-3673 (2002).

16. http://www-ssc.igpp.ucla.edu/dawn/spacecraft.html

17. http://dawn.jpl.nasa.gov/mission/index.asp

18. Tajmar, M., Gonzalez, J., and Hilgers, A., "Modeling of Spacecraft-Environment Interactions on SMART-1," AIAA Paper No. 2000-3526, *36th Joint Propulsion Conference and Exhibit*, Huntsville, Alabama, July 16-19, 2000.

19. Polk, J. E., Goebel, D. M., Snyder, J. S., Schneider, A. C., Johnson, L. K., Sengupta, A., "Performance and Wear Test Results for a 20 kW-Class Ion Engine with Carbon-Carbon Grids," AIAA Paper No. 2005-4393 (2005).

20. Sengupta, A., "Experimental and Analytical Investigation of a Ring Cusp Ion Thruster: Discharge Chamber and Performance," Ph. D. dissertation, University of Southern California, California, 2005.

21. Rovey, J. L., Gallimore, A. D., and Herman, D. A., "Potential Structure and Propellant Flow Rate Theory for Ion Thruster Discharge Cathode Erosion," IEPC-2005-022, 29th International Electric Propulsion Conference, Princeton University, October 31-November 4, 2005.

22. Herman, D. A., and Gallimore, A. D., "Discharge Chamber Plasma Potential Mapping of a 40-cm NEXT-type Ion Engine," AIAA Paper No. 2005-4251 (2005).

23. http://www.nasa.gov/centers/glenn/about/history/ipsworks.html

24. Goebel, D. M., Wirz, R. E., and Katz, Ira, "Analytical Ion Thruster Discharge Performance Model," AIAA Paper No. 2006-4486 (2006).

25. http://www.nasa.gov/centers/glenn/about/fs21grc.html

26. Goebel, D. M., Polk, J., and Sengupta, A., "Discharge Chamber Performance of the NEXIS Ion Thruster," AIAA Paper No. 2004-3813 (2004).

27. Rovey, J. L., and Gallimore, A. D., "Design and Operation of a Multiple-Cathode, High-Power, Rectangular Discharge Chamber," AIAA Paper No. 2005-4407, *41st Joint Propulsion Conference and Exhibit*, Tucson, Arizona, July 10-13, 2005.

28. Wirz, R., Goebel, D., "Ion Thruster Discharge Performance per Magnetic Field Topography," AIAA Paper No. 2006-4487 (2006).

29. Herman, D. A., and Gallimore, A. D., "Discharge Chamber Plasma Structure of a 40-cm NEXT-type Ion Engine," AIAA Paper No. 2005-4250 (2005).

30. Yount, R. A., "Plasma Uniformity of a 13-cm XIPS Thruster," M.S. Thesis, California Polytechnic State University, San Luis Obispo, CA, 2005

31. Jameson, K. K., "Development and Testing of a 13 cm XIPS Thruster," M.S. Thesis, California Polytechnic State University, San Luis Obispo, CA, 2003.

32. Martin, O., and Victor, A., "Operation of the HVEC Cryopump Vacuum Chamber and Resistojet Test," Senior Project, California Polytechnic State University, San Luis Obispo, CA, 2001.

33. Cuneo, Anthony, "Design and Construction of a Bell Jar Hoist," Senior Project, California Polytechnic State University, San Luis Obispo, CA, 2003.

# APPENDIX A: AXIAL MAGNETIC STRENGTH PLOTS

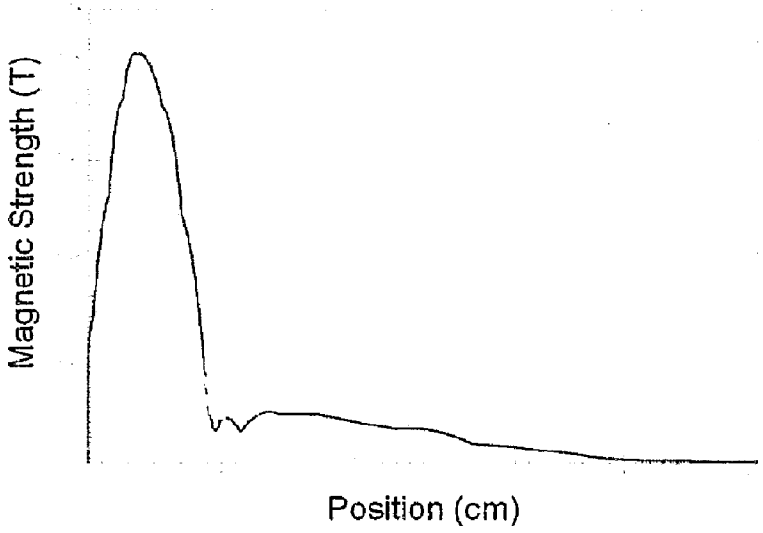


Figure 57 - MG 1 Axial Magnetic Strength

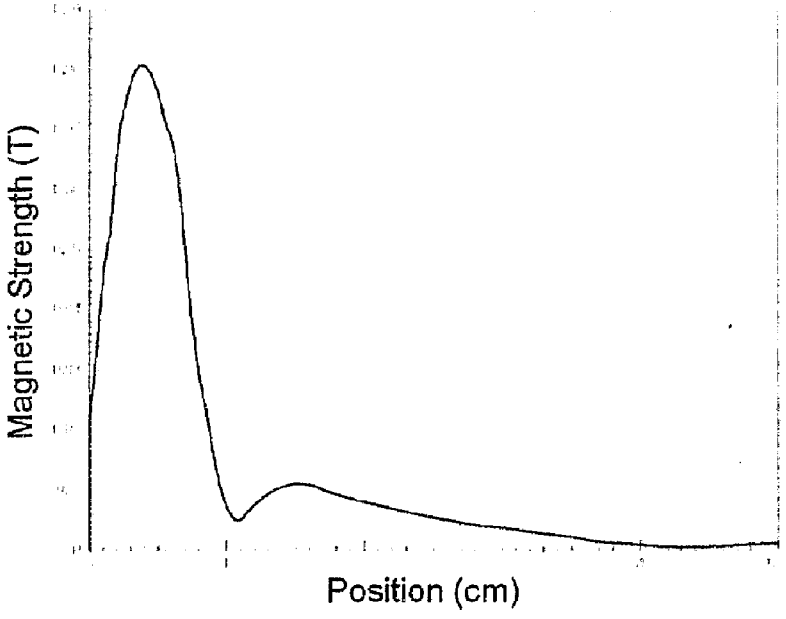


Figure 58 - MG 2 Axial Magnetic Strength

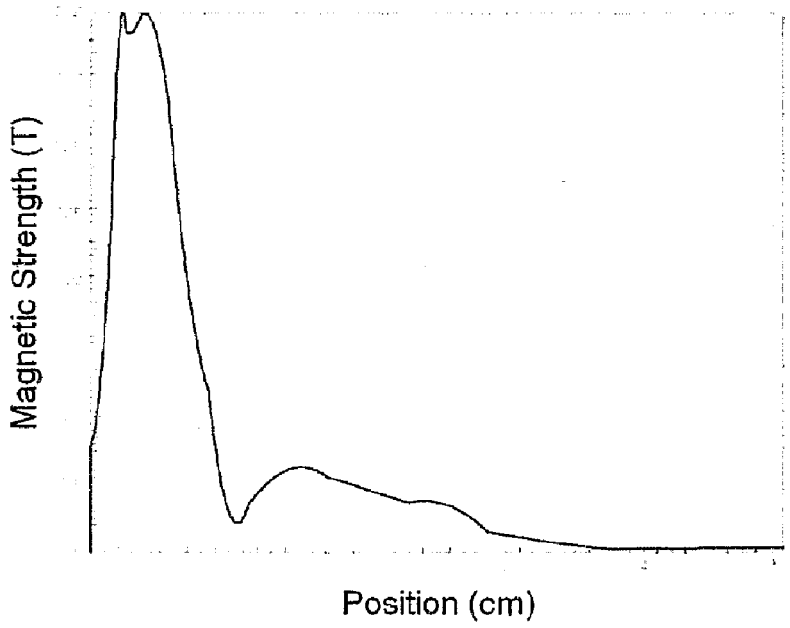


**Figure 59 - MG 4 Axial Magnetic Strength**

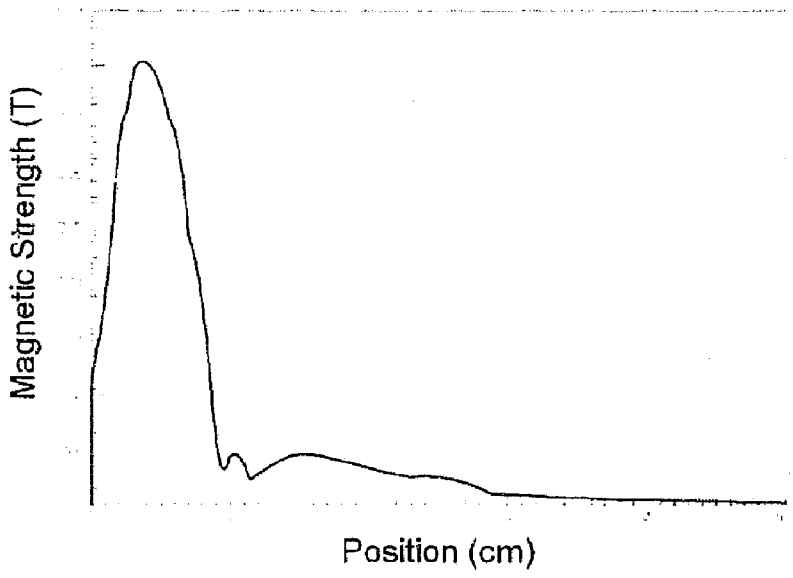


**Figure 60 - MG 5 Axial Magnetic Strength**